

DTIC FILE COPY

(4)

AD-A201 118

AFGL-TR-88-0200

UV Background Calculations: Rayleigh Scattered
and Dayglow Backgrounds from 1200 to 3000 A

D. J. Strickland
R. P. Barnes

Computational Physics, Inc.
P.O. Box 360
Annandale, VA 22003

and

D. E. Anderson, Jr.

E. O. Hulburt Center for Space Research
Naval Research Laboratory
Washington, DC 20375

24 August 1988

Scientific Report No. 1

Approved for public release; distribution unlimited.

AIR FORCE GEOPHYSICS LABORATORY
AIR FORCE SYSTEMS COMMAND
UNITED STATES AIR FORCE
HANSCOM AIR FORCE BASE, MASSACHUSETTS 01731


DTIC
ELECTE
NOV 21 1988
S D E

88 11 21 009

"This technical report has been reviewed and is approved for publication"



CHARLES A. FORSBERG
Contract Manager



ROBERT E. HUFFMAN
Branch Chief

FOR THE COMMANDER



ROBERT A. SKRIVANEK
Division Director

This report has been reviewed by the ESD Public Affairs Office (PA) and is releasable to the National Technical Information Service (NTIS).

Qualified requestors may obtain additional copies from the Defense Technical Information Center. All others should apply to the National Technical Information Service.

If your address has changed, or if you wish to be removed from the mailing list, or if the addressee is no longer employed by your organization, please notify AFGL/DAA, Hanscom AFB, MA 01731. This will assist us in maintaining a current mailing list.

Do not return copies of this report unless contractual obligations or notices on a specific document requires that it be returned.

UNCLASSIFIED

SECURITY CLASSIFICATION OF THIS PAGE

REPORT DOCUMENTATION PAGE				Form Approved OMB No. 0704-0188	
1a. REPORT SECURITY CLASSIFICATION UNCLASSIFIED			1b. RESTRICTIVE MARKINGS N/A		
2a. SECURITY CLASSIFICATION AUTHORITY			3. DISTRIBUTION/AVAILABILITY OF REPORT Approved for public release; distribution unlimited		
2b. DECLASSIFICATION/DOWNGRADING SCHEDULE N/A					
4. PERFORMING ORGANIZATION REPORT NUMBER(S) None			5. MONITORING ORGANIZATION REPORT NUMBER(S) AFGL-TR-88-0200		
6a. NAME OF PERFORMING ORGANIZATION Computational Physics, Inc.		6b. OFFICE SYMBOL (If applicable)		7a. NAME OF MONITORING ORGANIZATION Air Force Geophysics Laboratory	
6c. ADDRESS (City, State, and ZIP Code) P.O. Box 360 Annandale, VA. 22003			7b. ADDRESS (City, State, and ZIP Code) Hanscom Air Force Base Bedford, MA. 01731-5000		
8a. NAME OF FUNDING/SPONSORING ORGANIZATION Air Force Geophysics Lab.		8b. OFFICE SYMBOL (If applicable) LIU		9. PROCUREMENT INSTRUMENT IDENTIFICATION NUMBER MIPR- FY7121-88-00004	
8c. ADDRESS (City, State, and ZIP Code) Hanscom Air Force Base Bedford, MA. 01731-5000			10. SOURCE OF FUNDING NUMBERS		
PROGRAM ELEMENT NO. 63220C		PROJECT NO. S321		TASK NO. S32106 WORK UNIT ACCESSION NO S3210603	
11. TITLE (Include Security Classification) UV Background Calculations: Rayleigh Scattering and Dayglow Backgrounds from 1200 to 3000A					
12. PERSONAL AUTHOR(S) D.J. Strickland, R.P. Barnes and D.E. Anderson, Jr.*					
13a. TYPE OF REPORT Scientific Report #1		13b. TIME COVERED FROM 1/88 TO 4/88		14. DATE OF REPORT (Year, Month, Day) 24 august 1988	
15. PAGE COUNT 48					
16. SUPPLEMENTARY NOTATION * E.O. Hulburt Ctr for Space Research, Naval Research Lab, Washington, DC 20375					
17. COSATI CODES			18. SUBJECT TERMS (Continue on reverse if necessary and identify by block number)		
FIELD	GROUP	SUB-GROUP	Ultraviolet; UV; background; dayglow; Rayleigh scattering; limb		
0401	- 170502				
19. ABSTRACT (Continue on reverse if necessary and identify by block number)					
<p>An optical backgrounds model is discussed which calculates synthetic spectra of the dayglow and Rayleigh scattered sunlight for any satellite altitude and look direction. Spectra may be generated from EUV to near IR wavelengths. Integrations may be performed over wavelength and look angle (for field-of-view averaging) for direct comparison with observations. Limb profiles are presented in 100 A bands from 1400 to 3000 A in units of megaRayleighs A^{-4} and $Watts/cm^2/sr^{-1}$. These profiles combine dayglow and Rayleigh scattered sunlight and show how the brightness varies over the tangent altitude range 300 to 0 km. Dayglow results are presented for high and low solar activity. There can be more than an order of magnitude variation in dayglow brightness at tangent altitudes above 200 km from low to high activity. We also present limb profiles of Rayleigh scattered sunlight showing the effect of changing the sun's azimuth. For a chosen solar zenith angle of 60°, variations of more than 50% occur as the sun's azimuth changes from 0° to 90°.</p>					
20. DISTRIBUTION/AVAILABILITY OF ABSTRACT <input checked="" type="checkbox"/> UNCLASSIFIED/UNLIMITED <input type="checkbox"/> SAME AS RPT <input type="checkbox"/> DTIC USERS			21. ABSTRACT SECURITY CLASSIFICATION UNCLASSIFIED		
22a. NAME OF RESPONSIBLE INDIVIDUAL Dr. R.W. Eastes			22b. TELEPHONE (Include Area Code) (617) 377-3208		22c. OFFICE SYMBOL AFGL/LIU

TABLE OF CONTENTS

Figure Captions.....	p.	iv
Preface.....	p.	vii
1. Introduction.....	p.	1
2. Dayglow Model.....	p.	1
3. Rayleigh Scattering Model.....	p.	2
4. Spectral Models.....	p.	3
5. Physical and Observing Conditions.....	p.	4
6. Volume Emission Rates.....	p.	5
7. Synthetic Spectra.....	p.	6
8. Limb Profiles.....	p.	14
9. Azimuthal Effects.....	p.	14
10. Future Direction.....	p.	38
11. Acknowledgments.....	p.	39
12. References.....	p.	39

Accession For	
NTIS GRA&I	<input checked="" type="checkbox"/>
DTIC TAB	<input type="checkbox"/>
Unannounced	<input type="checkbox"/>
Justification	
By _____	
Distribution/	
Availability Codes	
Dist	Avail and/or Special
A-1	



FIGURE CAPTIONS

1. Dayglow volume emission rates for high solar activity.....p.	7
2. Rayleigh scattering volume emission rates.....p.	8
3. Dayglow spectra for tangent altitudes of 300 and 250 km for high solar activity and a solar zenith angle of 30°p.	9
4. Similar to Figure 3 except for altitudes of 200 and 150 km.....p.	10
5. Similar to Figure 3 except for altitudes of 100 and 80 km.....p.	11
6. Similar to Figure 3 except for altitudes of 60 and 40 km.....p.	12
7. Similar to Figure 3 except for altitudes of 20 and 0 km.....p.	13
8. Spectra for Rayleigh scattering at a solar zenith angle of 30°p.	15
9. Limb profiles over the wavelength interval 1400 - 1500 A for high and low solar activity and limb resolutions of 3, 10 and 30 km.....p.	16
10. Similar to Figure 9 except from 1500 to 1600 A.....p.	17
11. Similar to Figure 9 except from 1600 to 1700 A.....p.	18
12. Similar to Figure 9 except from 1700 to 1800 A. Rayleigh scattering begins to appear in this band but has not been included in this figure.....p.	19
13. Similar to Figure 12 except from 1800 to 1900 A.....p.	20
14. Similar to Figure 12 except from 1900 to 2000 A.....p.	21
15. Similar to Figure 9 except from 2000 to 2100 A with the addition of Rayleigh scattering.....p.	22
16. Similar to Figure 15 except from 2100 to 2200 A.....p.	23
17. Similar to Figure 15 except from 2200 to 2300 A.....p.	24
18. Similar to Figure 15 except from 2300 to 2400 A.....p.	25
19. Similar to Figure 15 except from 2400 to 2500 A.....p.	26
20. Similar to Figure 15 except from 2500 to 2600 A.....p.	27
21. Similar to Figure 15 except from 2600 to 2700 A.....p.	28
22. Similar to Figure 15 except from 2700 to 2800 A.....p.	28
23. Similar to Figure 15 except from 2800 to 2900 A.....p.	30
24. Similar to Figure 15 except from 2900 to 3000 A.....p.	31
25. Limb profiles from Figs. 15 and 24 shown in greater detail around the 100 km tangent point.....p.	32
26. Geometry illustrating scattering angle θ in relation to sun's azimuth ϕp.	34
27. Limb profiles showing the effect of changing the sun's azimuth for the wavelength interval 2000-2100 A. A given angle refers to the angle between the look and sun vectors.....p.	35

28. Similar to Fig. 26 except for the interval
2400-2500 A.....p. 36
29. Similar to Fig. 26 except for the interval
2900-3000 A.....p. 37

Accession For	
NTIS GRA&I	<input checked="" type="checkbox"/>
DTIC TAB	<input type="checkbox"/>
Unannounced	<input type="checkbox"/>
Justification	
By	
Distribution/	
Availability Codes	
Dist	Avail and/or Special
A-1	

PREFACE

Ultraviolet sensors for missile defense must be developed based on accurate knowledge of the radiative environment or background within which such sensors will be used. This report represents a beginning effort to provide such accurate knowledge by presenting the results of model calculations of the expected backgrounds using the current understanding of upper atmospheric and ionospheric physics. The effort is a part of the Ultraviolet Phenomenology work supported by SDIO/T-SN, Dr. Barry Katz, through Dr. Robert E. Huffman at AFGL.

These background levels are suitable for use in planning ultraviolet background measurements on SDIO observational programs such as STARLAB, IBSS, etc. Along with currently available material, this information has been made available to the mentioned SDIO programs through Experimenter's Working Groups and more widely through WPD 32.1 Reviews and Phenomenology Steering and Analysis Group (PSAG) meetings.

Model calculations such as these will also be used in the critical data analysis and review planned for new observational data. The ultimate goal is to provide the best available models of the backgrounds and its variability to SDIO users for scene generation, systems architecture, and sensor development applications.

Until new data are available, theoretical treatments of regions with complicated spectral structure will continue. For this purpose, use continues to be made of existing AFGL data bases from the AIRS UV imager on the Polar BEAR satellite and the S3-4 VUV Backgrounds satellite experiment and other existing data.

1. INTRODUCTION

Computational Physics, Inc., working jointly with the Upper Atmospheric Physics Branch of the Space Science Division of NRL, has developed optical background models for the dayglow and Rayleigh scattering of sunlight. The wavelength range presently goes from about 800 A to 10,000 A (this range for the dayglow and 2010 to 8000 A for Rayleigh scattering). Key quantities calculated by the models are synthetic spectra in both megaRayleighs A^{-1} and $\mu\text{Watts cm}^{-2} \text{sr}^{-1} \mu^{-1}$ for any observing altitude and look direction of interest. From these, we further obtain limb profiles by integrating these spectra over specified wavelength and look angle intervals and then joining the two components (dayglow and Rayleigh scattering) together. The integrations allow for convolution with instrument response functions so that direct comparisons can be made with observations. This report will describe the various parts of the models and then present results demonstrating present capabilities. We refer the reader in advance to Table 1 which summarizes observing and physical conditions being addressed. (Section 5 is dedicated to this topic.)

2. DAYGLOW MODEL

Our dayglow model provides first principles calculations of photoelectron transport, chemistry and photon transport. Calculated quantities of interest are:

1. photoelectron spectra
2. volume excitation rates
3. ion and neutral densities
4. intensities.

Intensities are provided by codes LIMB and LIMB1304. LIMB is a major code developed over the past three years which calculates intensities for a variety of features. The geometry is spherical and the observing point may be either above or within the emission region. Intensities are specified as functions of look angle which may range from 0° (zenith) to 180° . The code contains a "smart" integrator which examines the integrand along the line-of-sight, sets up integration intervals and then performs Gaussian integrations. Features and systems currently handled by LIMB include the O lines at 1356 A, 2972 A, 5577 A, 6300 A, 7774 A and 8446 A, the O^+ 834 A triplet, other lines such as NI 1493, O^+ 2471 A and O^+ 7320 A and finally the band systems N_2 LBH, N_2 VK, N_2 2PG, N_2 1PG, NO γ and N_2^+ 1N. The volume emission rates for OI 1356 A and O^+ 834 A require special attention because of multiple scattering. The needed

transport calculations are performed by code DSDA prior to running LIMB.

LIMB1304 is also a major code recently developed to calculate OI 1304 A limb profiles from source functions obtained by a rigorous frequency redistribution description.⁽⁴⁾ Profiles are obtained for each of the triplet lines and for both sources (solar 1304 A photons and photoelectron impact excitation).

3. RAYLEIGH SCATTERING MODEL

Our Rayleigh scattering model provides a first-principles calculation of multiple scattering from 2010 A to 8000 A. The model accounts for pure absorption by O₂ and O₃ and allows for a range of surface conditions (different albedos and surface heights). Rayleigh scattered sunlight begins to appear above the dayglow background around 1750 A. Below this wavelength, pure absorption by O₂ prevents the sun's radiation from penetrating deep enough into the atmosphere to produce any measurable backscatter. Between about 1750 and 2000 A, the backscattered spectrum rises about three orders of magnitude and has a high degree of structure caused by O₂ Schumann-Runge band absorption. Our model does not presently address this region because of the severe computational difficulties associated with the structure. Work is underway, however, to provide estimates of radiance limits over selected band intervals within this region.

The model is based on an isotropic formulation that performs a one-time matrix inversion to determine the radiation field for all angles of interest to the external photon source and for a given model atmosphere.⁽⁵⁾ For Rayleigh scattering, the results agree to high accuracy with a detailed Monte Carlo model of the molecular scattering.⁽⁶⁾ When aerosols are present, the model reproduces the Monte Carlo results to 10% or better.⁽⁷⁾ The model assumes plane parallel geometry so its applicability is limited to solar zenith angles of less than approximately 95°. Tests indicate, however, that up to 95°, the results are accurate.⁽⁸⁾

To examine azimuthal effects referenced to the sun direction, the radiation field is separated into a singly scattered (SS) and multiply scattered (MS) component. The MS component is treated as isotropic, which is a good approximation for monochromatic scattering and the SS component is scaled by the Rayleigh phase function appropriate to the observing conditions. In the presence of aerosols or clouds, the Mie phase function is used. The present report addresses Rayleigh scattering only. At wavelengths in excess of 320 nm, the

effects of aerosols and clouds can be important and may be considered in a future report.

Volume emission rates calculated by the above model are read into code RAYLIMB which then calculates limb radiances in units of either megaRayleighs A^{-1} or $\mu Watts\ cm^{-2}\ sr^{-1}$. The possible range of tangent altitudes is from approximately 100 km to -6370 km (-6370 refers to nadir viewing). RAYLIMB has been developed over the past year and has its origins in code LIMB.

4. SPECTRAL MODELS

The outputs from both of the above described models are respectively read into codes SYNSPEC and RAYSPEC. SYNSPEC is a major code written in IDL which generates normalized synthetic spectra for the above mentioned band systems, scales them by the calculated total system limb intensities and adds all such scaled spectra on a common wavelength grid. For LBH, pure absorption by O_2 is correctly accounted for as a function of wavelength. Emission lines are added at their appropriate wavelengths after smoothing which is consistent with the chosen resolution. Routines of R. Conway are employed to obtain the normalized spectra for LBH, 2PG and VK. These routines return the spectra at the user specified resolution, rotational temperature and wavelength grid spacing. A routine provided by R. McCoy is used to generate the normalized spectrum for the NO γ bands. The spectrum contains the same level of detail as those of Conway. The remaining systems are given a simpler description. Each such spectrum is treated as a series of lines in place of its bands and appropriately smoothed for the specified resolution.

RAYSPEC is also written in IDL but is a much simpler code. The wavelength grid is composed of those wavelengths for which limb profiles were obtained by RAYLIMB. It basically takes the family of limb profiles calculated by RAYLIMB, places them into a two dimensional array (versus wavelength and tangent altitude) and proceeds to plot spectra for user specified tangent altitudes.

Important improvements have recently been made to both SYNSPEC and RAYSPEC. It is now possible to integrate the spectra over wavelength and look angle to obtain limb profiles for either simulation of or comparisons with measurements. Many wavelength intervals are permitted within each run for which the user specifies beginning and ending wavelengths. The integration over look angle gives field-of-view (FOV) averaged profiles for either a circular or rectangular FOV. Finally, the resulting profiles from the two codes may be added together. Results will follow

showing the combined profiles for several integrated wavelength intervals and three circular FOVs.

5. PHYSICAL AND OBSERVING CONDITIONS

The dayglow results to follow are sensitive to solar activity. At tangent altitudes such as 300 to 400 km, the dayglow can increase by more than an order of magnitude going from low to high activity. This is due to the increase in the photoelectron population which is the main source of the dayglow and to increased atmospheric densities accompanying the increased exospheric temperature. At lower tangent altitudes, the increase will be on the order of two to three. The parameter which specifies solar activity in our model is the 10.7 cm flux designated $F_{10.7}$. Results will follow for values of 70 and 250 which reflect low and high activity. This parameter is used in an empirical relationship applied to each of the 800 or so lines in our solar spectrum. The relationship and the base spectrum come from Hinteregger.^(9, 10) $F_{10.7}$ is also a parameter appearing the MSIS 83 model⁽¹¹⁾ which is providing our model atmospheres in this work. [Two parameters are actually called for: an averaged value for the previous three months and a value for the previous day.]

The solar spectrum longward of 2000 Å is not sensitive to solar activity and consequently the same one is used in our Rayleigh scattering calculations for low and high activity.⁽¹²⁾ Results have been obtained for two solar zenith angles (SZA): 30° and 60°. The models presently handle angles up to about 100° for photoelectron produced emissions and 90° for Rayleigh scattering. The limit for Rayleigh scattering will likely be extended in future work. We will be presenting results for only the first of the two SZAs. This is because the background does not change significantly in going from 30° to 50° and because of the large number of figures involved.

Sixteen adjacent wavelength intervals have been selected for generating limb profiles. Each is 100 Å wide with the first starting at 1400 Å and the last ending at 3000 Å. Tangent altitude resolutions of 1, 3 and 10 km will be considered. This parameter refers to the interval seen on the limb and is determined by the satellite's altitude and FOV.

A resolution of 10 Å has been chosen for generating dayglow spectra. They have been placed on a uniform grid with a spacing of 2 Å. The spectra to follow begin at 1200 Å and include Hydrogen Lyman Alpha at 1216 Å and OI 1304 Å. Their limb profiles were calculated specifically for inclusion in this report but should be viewed in a somewhat qualitative sense. In

actuality, they vary with model atmosphere, solar activity, satellite altitude and SZA. The given results apply to small SZAs and to solar activity in the moderate range.

The limb profiles in this report will be given versus tangent altitude (300 to 0 km) rather than look direction. The advantage of this is that the profile is invariant with satellite altitude provided that the satellite is effectively above the emitting region. This will generally be the case except for HI 1216 A and possibly 1304 A. For the latter feature, the satellite altitude must be approximately 800 km or greater to be above the emitting region.

The following table summarizes the parameters discussed in this section.

Table 1. Parameters related to physical and observing conditions

PARAMETER	VALUE or REFERENCE
Solar spectrum (X-rays to 1000 A)	References 9 & 10
Solar spectrum (2000 - 3000 A)	Reference 12
Model Atmosphere	Reference 11
F10.7 (10^{-22} Watts cm^{-2} Hz^{-1})	70 and 250
Solar zenith angles	30° and 60°
Wavelength intervals	
Widths	100 A
Number	16
First	1400 - 1500 A
Last	2900 - 3000 A
Resolution on limb	3, 10 and 30 km
Spectral resolution (dayglow)	10 A
Grid spacing (dayglow)	2 A
Range of tangent altitudes	300 to 0 km

6. VOLUME EMISSION RATES

The key inputs to the limb codes discussed above are volume emission rates. In the case of the dayglow, the rates apply to discrete features, these being either atomic lines or systems of molecular bands. In the case of Rayleigh scattering, we are dealing effectively with continuum emission and thus may define the emission rate at any wavelength. Selected rates will follow

for both the dayglow and Rayleigh scattering to illustrate the striking contrast in altitude dependence which can occur from one rate to another.

Figure 1 gives rates for LBH, 2PG, VK, OI 1356 A and NI 1493 A as well as the densities of $O(^2P)$ and $O(^1S)$ and finally the NO density times 10^{-6} . The $O(^2P)$ and $O(^1S)$ densities give the emission features 2471 A and 2972 A when multiplied by their appropriate transition rates. The scaled NO density gives the fluorescence emission in the γ bands when multiplied by appropriately scaled g-factors. The results in the figure refer to high solar activity. Multiple scattering calculations were performed for OI 1356 A. The figure shows the emission rate before and after scattering. The applied NO density and needed g-factors come from McCoy.^(13, 14) Time dependent chemistry modeling was applied to VK, $O(^2P)$ and $O(^1S)$.

Figure 2 shows volume emission rates for Rayleigh scattering. The upper panel gives selected rates shortward of about 2500 A where pure absorption by O_3 and O_2 at the shorter wavelengths prevents the emission from penetrating into the lower atmosphere. The lower panel gives selected rates longward of 2500 A and shows the dramatic increase in emission at low altitudes as O_3 absorption decreases. The longest wavelength shown is 3053 A since interest in this report ends at about this wavelength. It is worth noting, however, that the emission rate near the surface continues to increase with increasing wavelength out to about 4000 A. Values in excess of 2×10^7 photons $cm^{-3} s^{-1} A^{-1}$ are obtained by our model longward of 3200 A.

7. SYNTHETIC SPECTRA

Separate spectra will follow for the dayglow and Rayleigh scattering. Their combined emissions will be shown in the next section in the form of limb profiles for given wavelength intervals and FOVs. Figures 3 - 7 give dayglow spectra at high solar activity for tangent altitudes of 300, 250, 200, 150, 100, 80, 60, 40, 20 and 0 km. Each figure displays spectra for two successive altitudes. The upper panel for any given figure covers the wavelength range 1200 to 2000 A while the lower panel goes from 2000 to 3000 A. The dominant features from 1200 to 2000 A are HI 1216 A, OI 1304 A, OI 1356 A and the system of LBH bands starting at 1273 A and continuing through the entire wavelength range. The dominant features modeled from 2000 to 3000 A are the NO γ , VK and 2PG systems and the lines O^* 2471 and OI 2972. LBH also contributes at short wavelengths within this region. We do not show spectra at low solar activity because of the quantity of information being presented. Low and

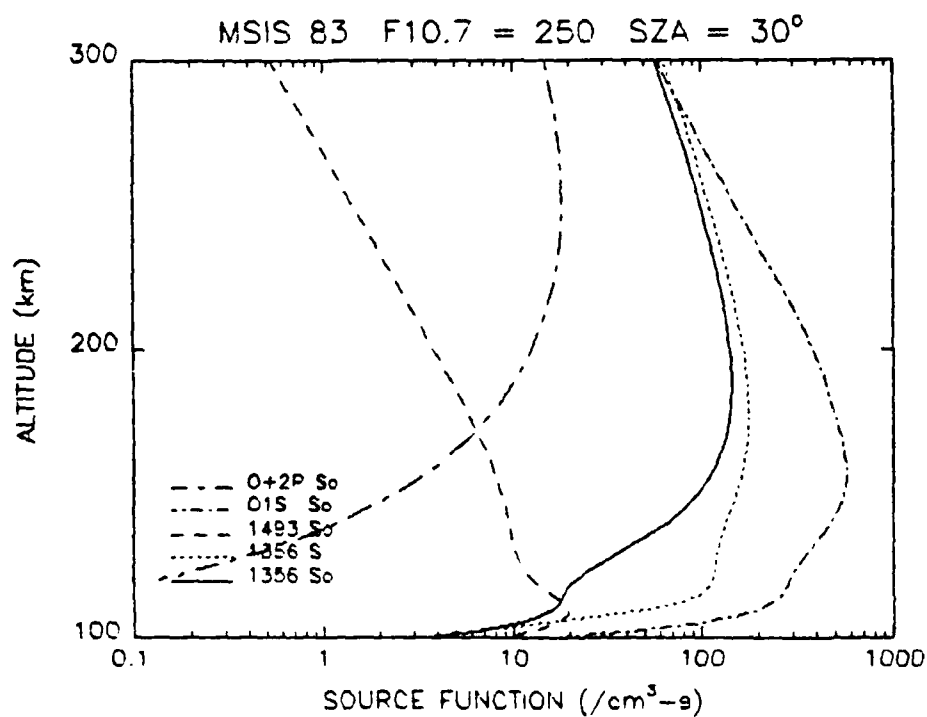
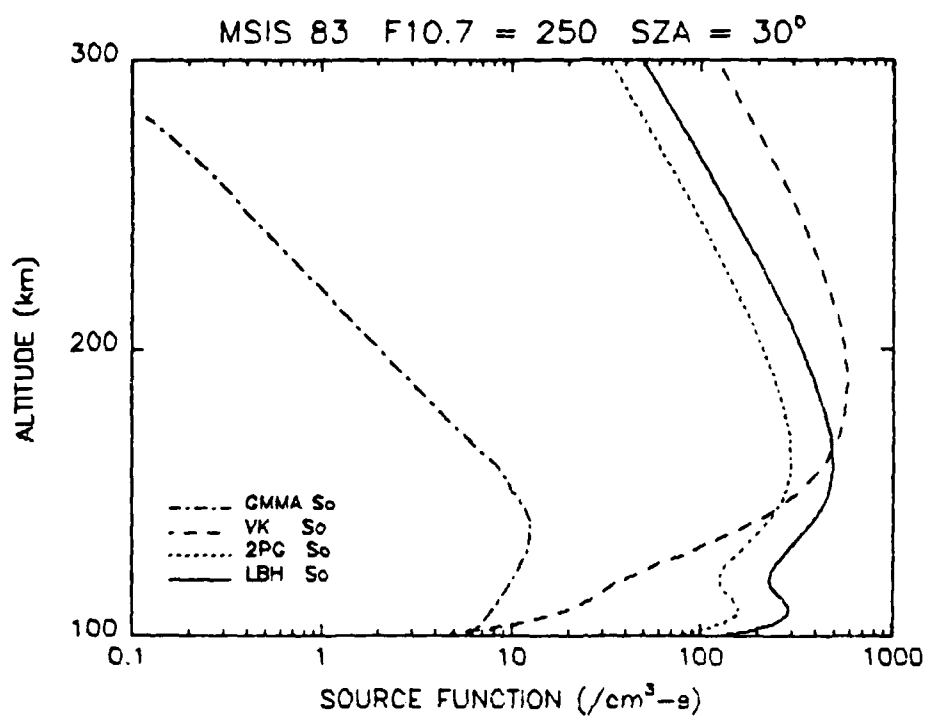


Figure 1. Dayglow volume emission rates for high solar activity

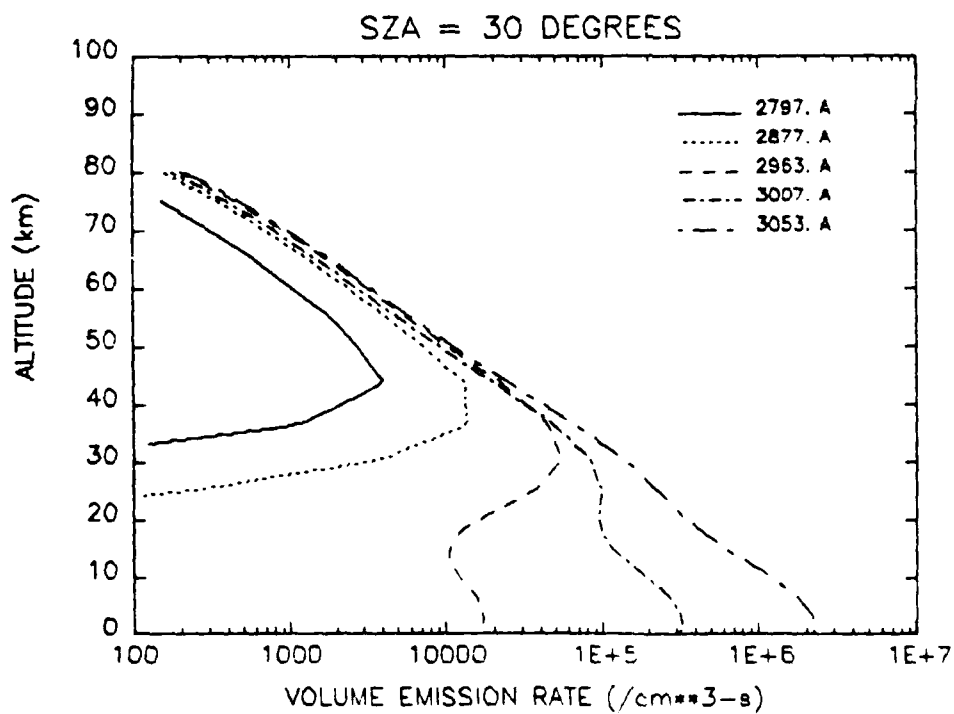
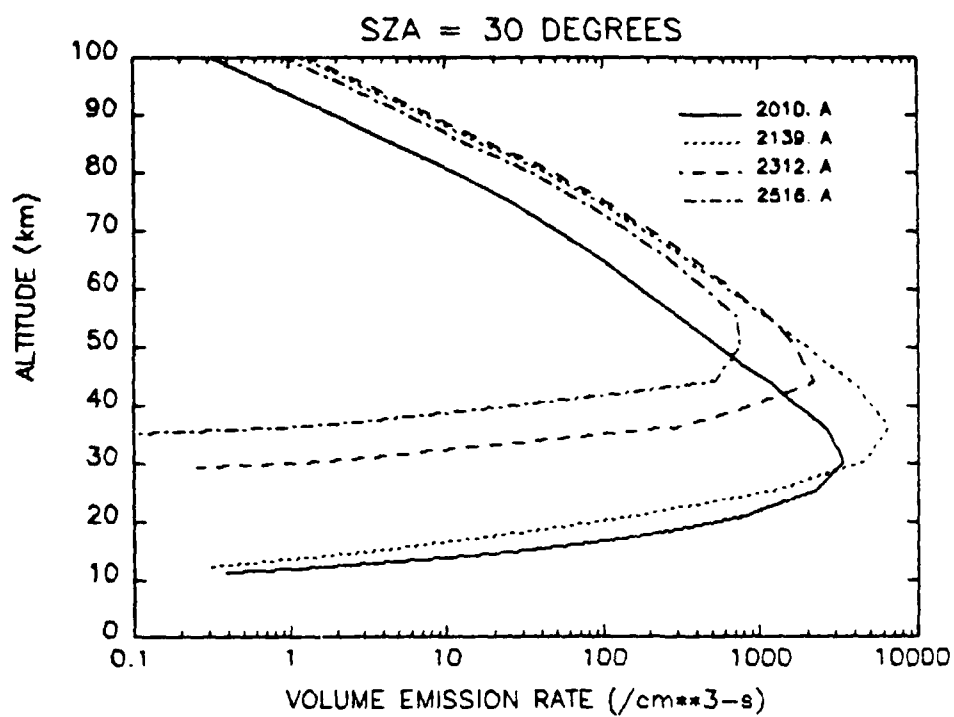


Figure 2. Rayleigh scattering volume emission rates

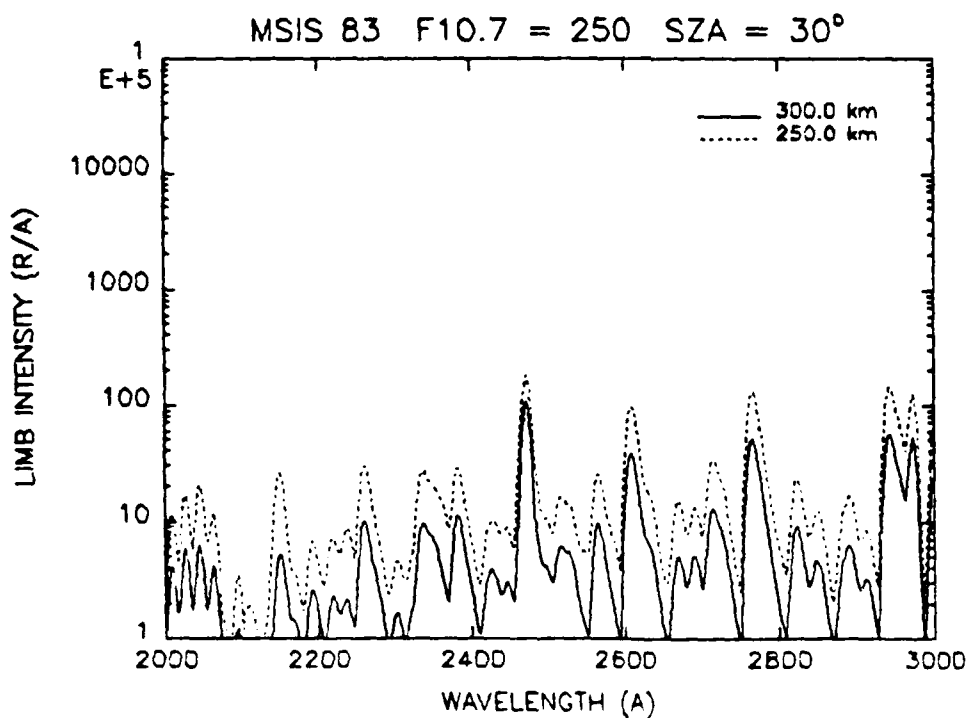
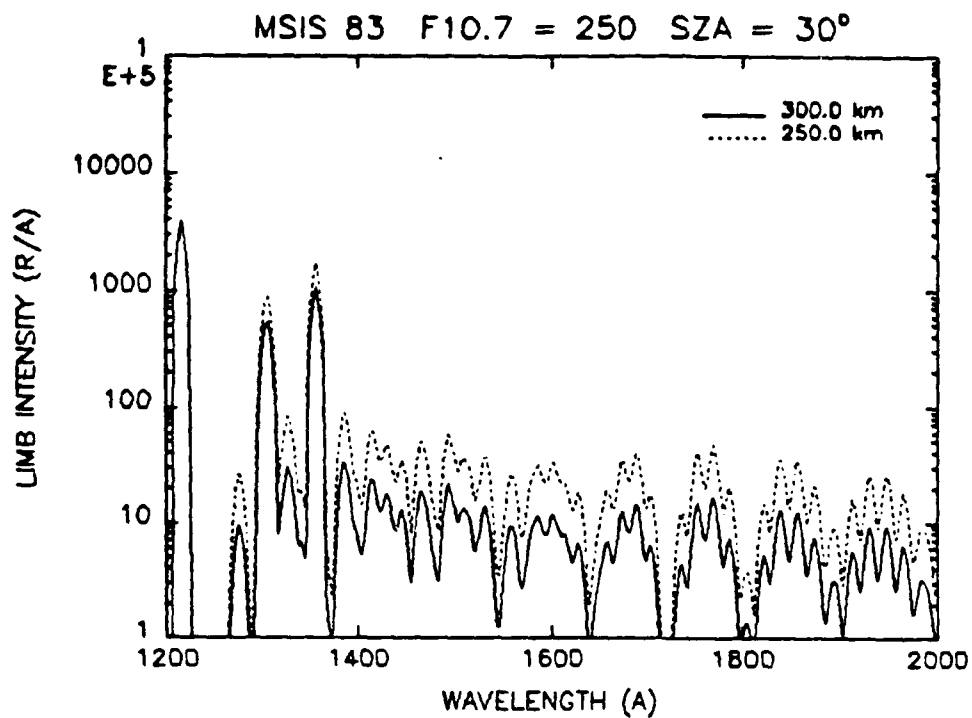


Figure 3. Dayglow spectra for tangent altitudes of 300 and 250 km for high solar activity and a solar zenith angle of 30°.

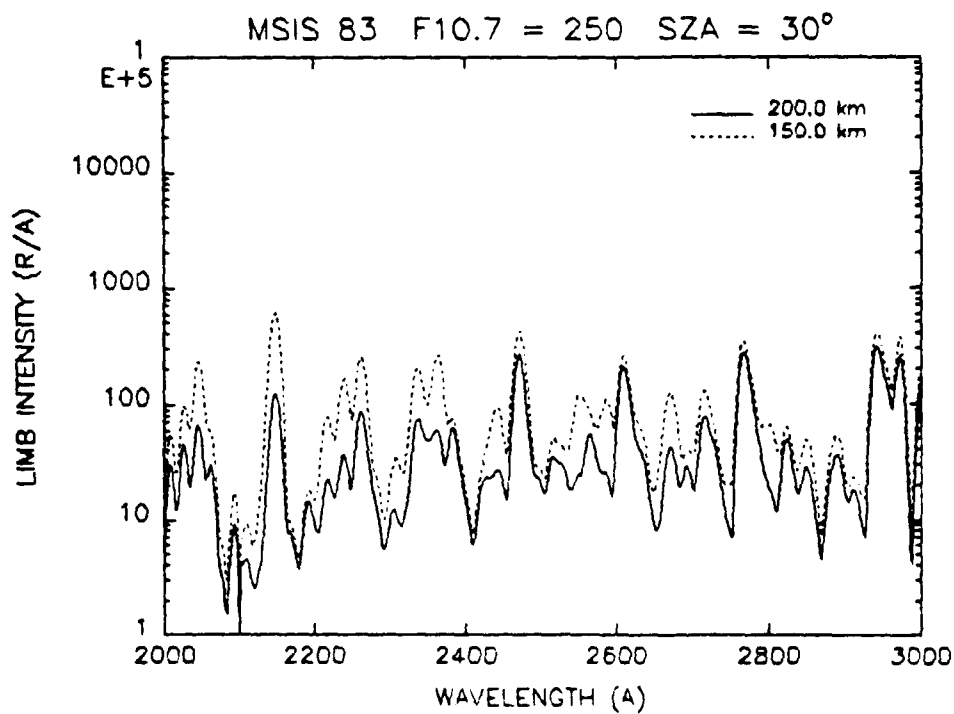
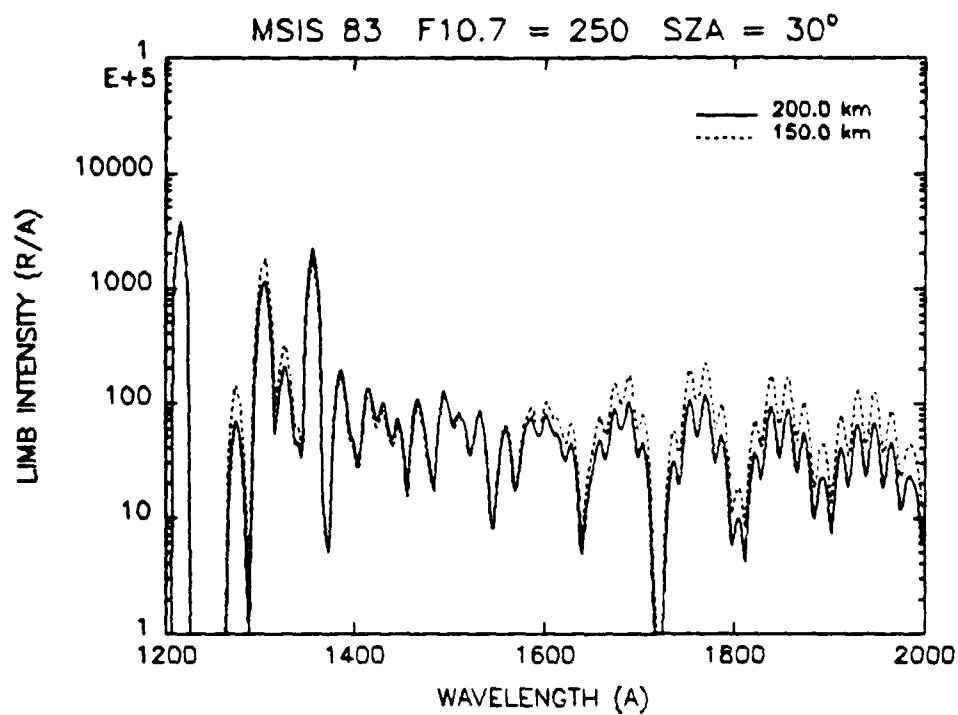


Figure 4. Similar to Figure 3 except for altitudes of 200 and 150 km

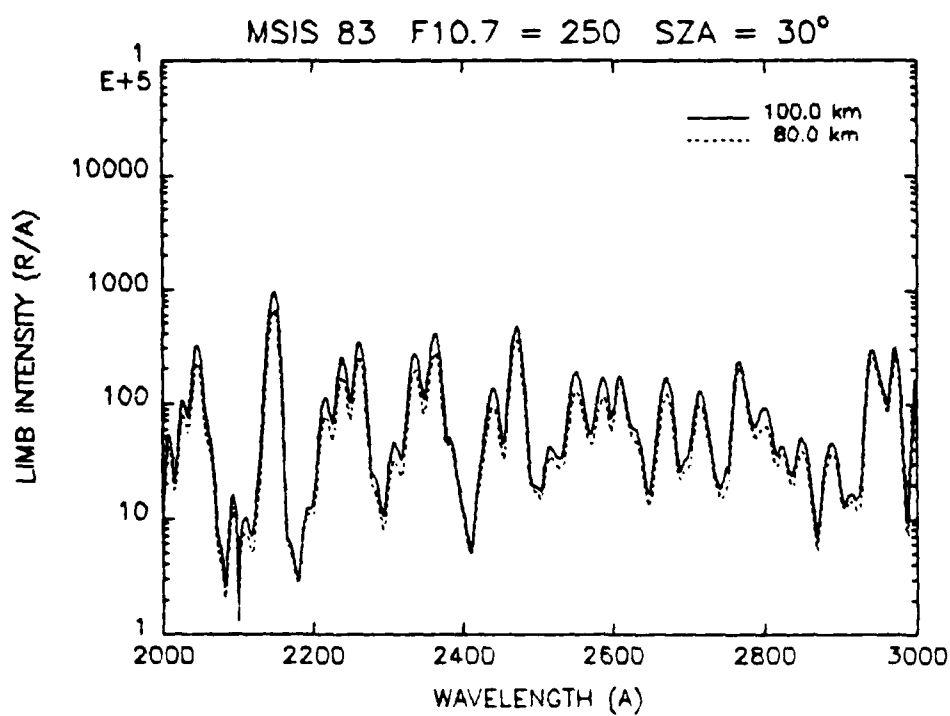
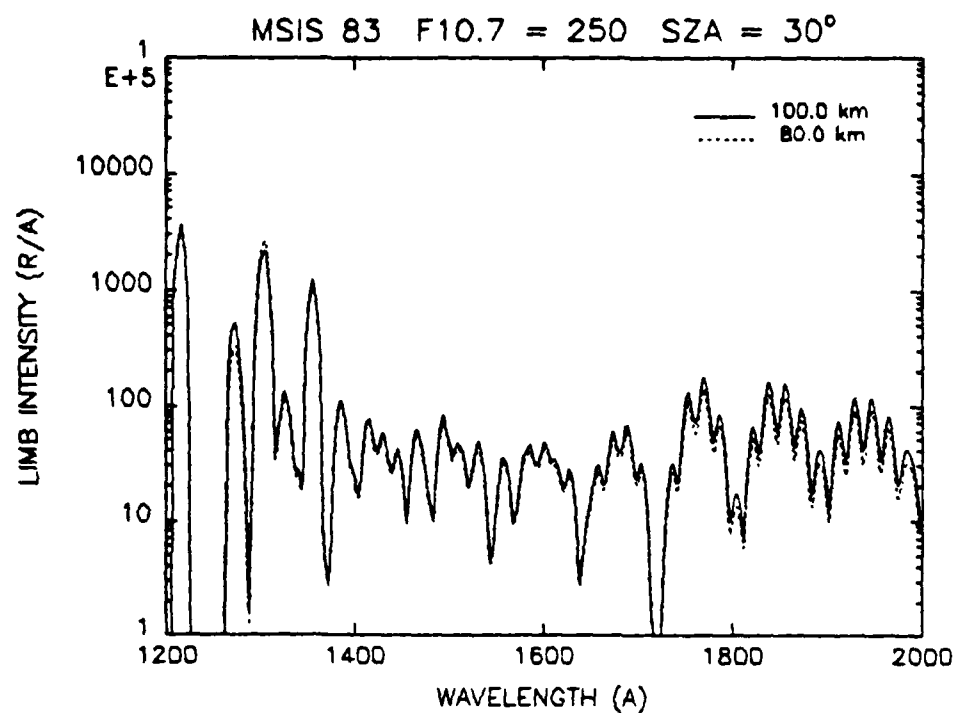


Figure 5. Similar to Figure 3 except for altitudes of 100 and 80 km

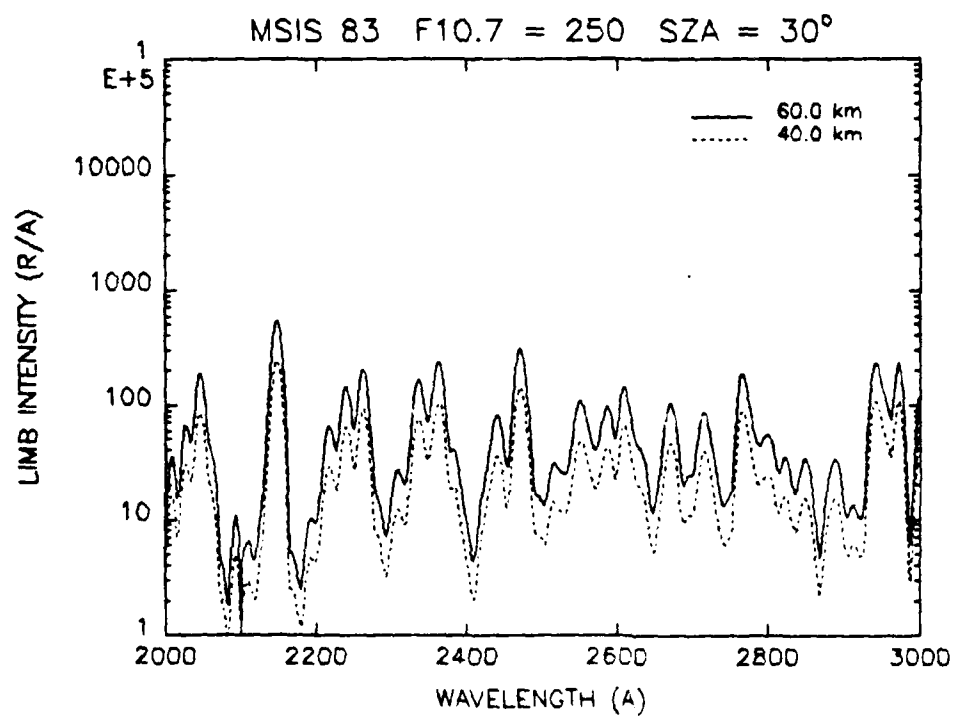
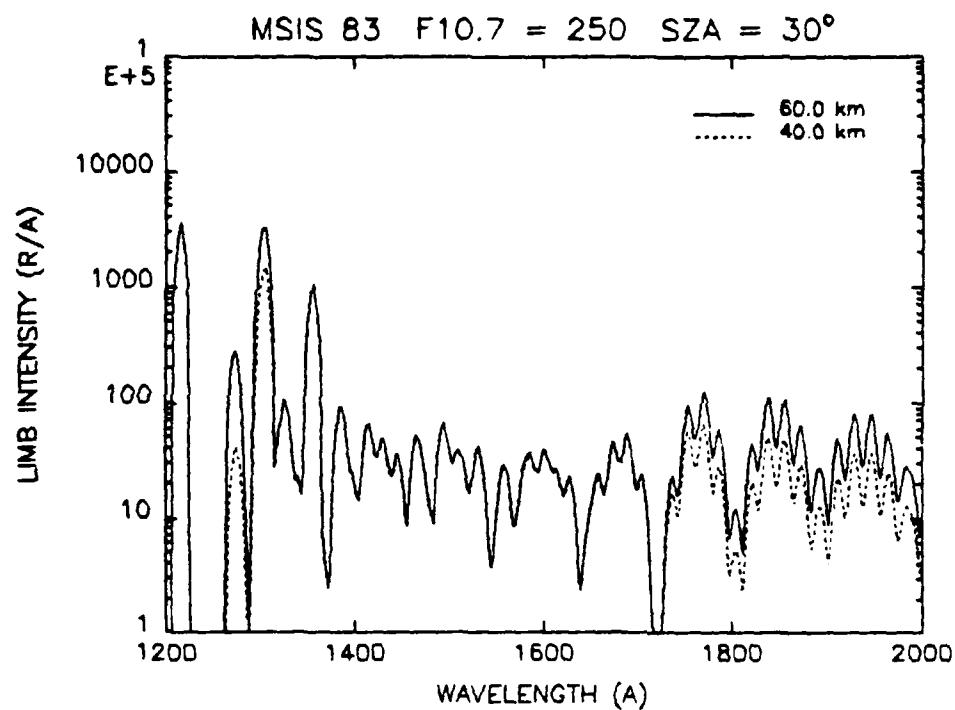


Figure 6. Similar to Figure 3 except for altitudes of 60 and 40 km

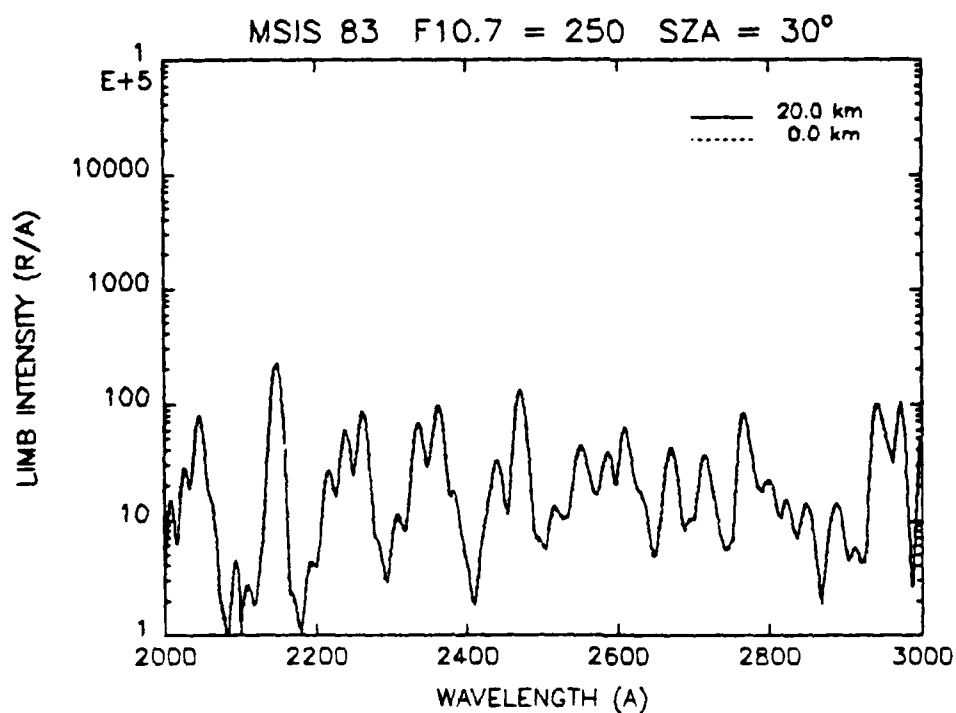
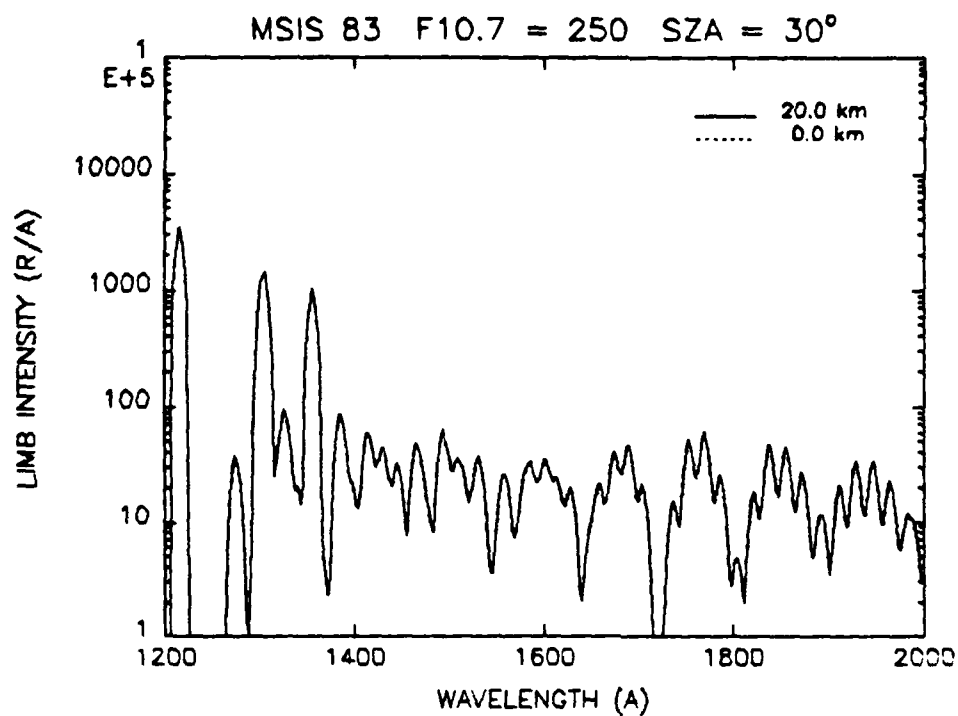


Figure 7. Similar to Figure 3 except for altitudes of 20 and 0 km

high activity results will, however, be presented in the next section in the form of limb profiles.

Figure 8 shows spectra for Rayleigh scattering. The chosen tangent altitudes are the same as above except that the first four have been deleted. Above 100 km, limb emission from Rayleigh scattering is insignificant compared to the dayglow. The structure in the displayed spectra from 2000 to 3500 Å is caused by O₃ absorption which peaks near 2500 Å. The rapid rise longward of 2800 Å results from the penetration of solar photons into the lower atmosphere as discussed in the previous section. This explains why there is much less rise at the larger tangent altitudes since for these, the line of sight does not penetrate to altitudes where the volume emission rate becomes large at wavelengths like 3000 Å (see Figure 2).

8. LIMB PROFILES

The spectra shown above appear within codes SYNSPEC and RAYSPEC as two dimensional arrays versus wavelength and tangent altitude. Limb profiles to follow were obtained by integrating these arrays over specified intervals in both variables. Integration over tangent altitude (actually over look angle in the code) provides field-of-view averaging for either circular or rectangular FOVs. Here, we chose circular FOVs to give the limb resolutions shown in Table 1 (3, 10 and 30 km). The respective limb profiles from SYNSPEC and RAYSPEC are placed on files and read into another code where they are joined for each wavelength interval. It is these profiles which we present here. We have selected sixteen intervals from 1400 to 3000 Å as discussed in Section 5. The next sixteen figures (Figures 9 - 24) show limb profiles for these intervals. The upper panel and lower panels in each figure respectively show the results in megaRayleighs and in $\mu\text{Watts cm}^{-2} \text{sr}^{-1}$. Each panel contains six profiles for the possible combinations of limb resolution and solar activity. The differences from one FOV averaged profile to the next are not distinguishable on the scale chosen for displaying the profiles. Thus, we include Figure 25 which shows the profiles from Figures 15 (2000-2100 Å) and 24 (2900-3000 Å) in greater detail around the 100 km tangent point to illustrate the effect of changing the FOV from 3 to 30 km resolution.

9. AZIMUTHAL EFFECTS

The Rayleigh scattering results presented above were obtained by assuming isotropic scattering. Actual scattering is

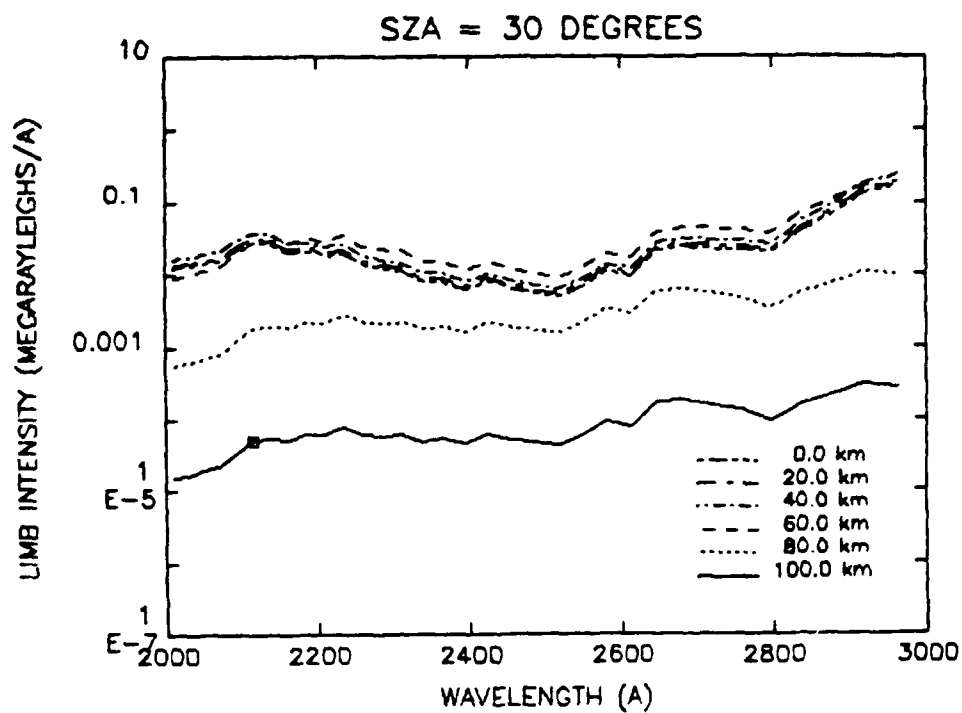


Figure 8. Spectra for Rayleigh scattering at a solar zenith angle of 30°

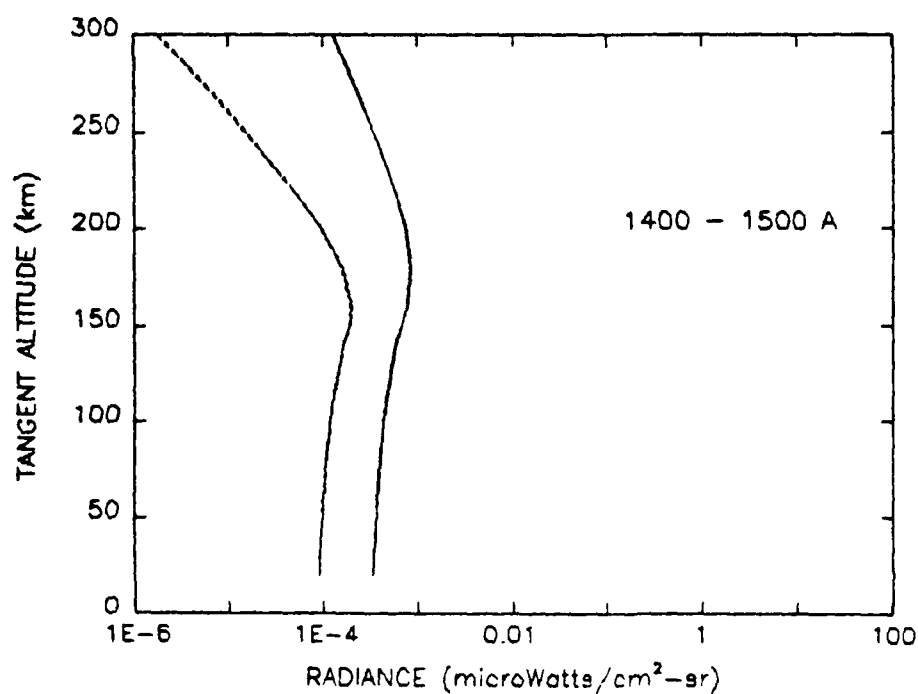
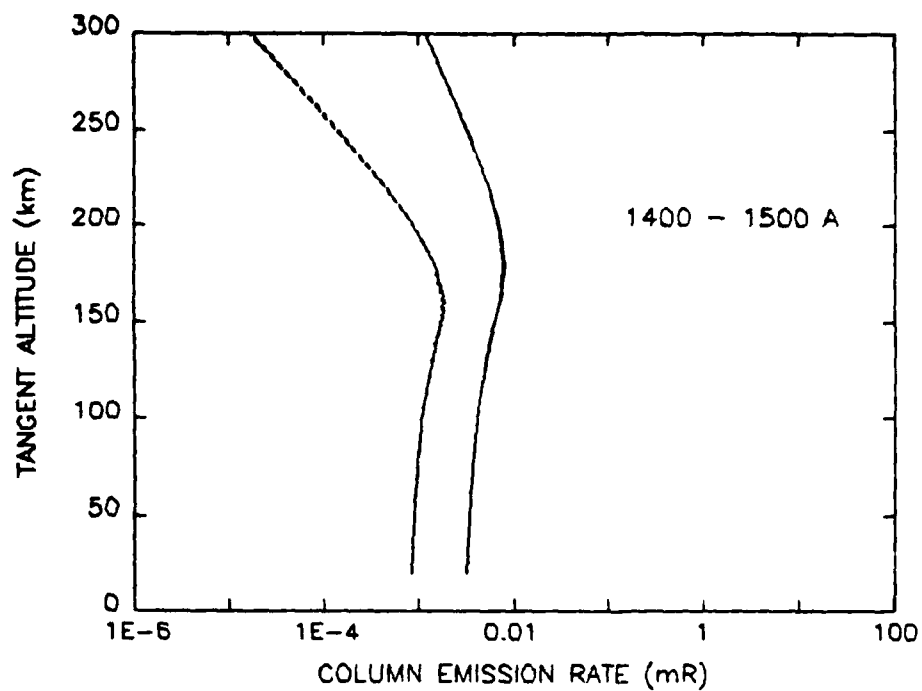


Figure 9. Limb profiles over the wavelength interval 1400 - 1500 Å for high and low solar activity and limb resolutions of 3, 10 and 30 km

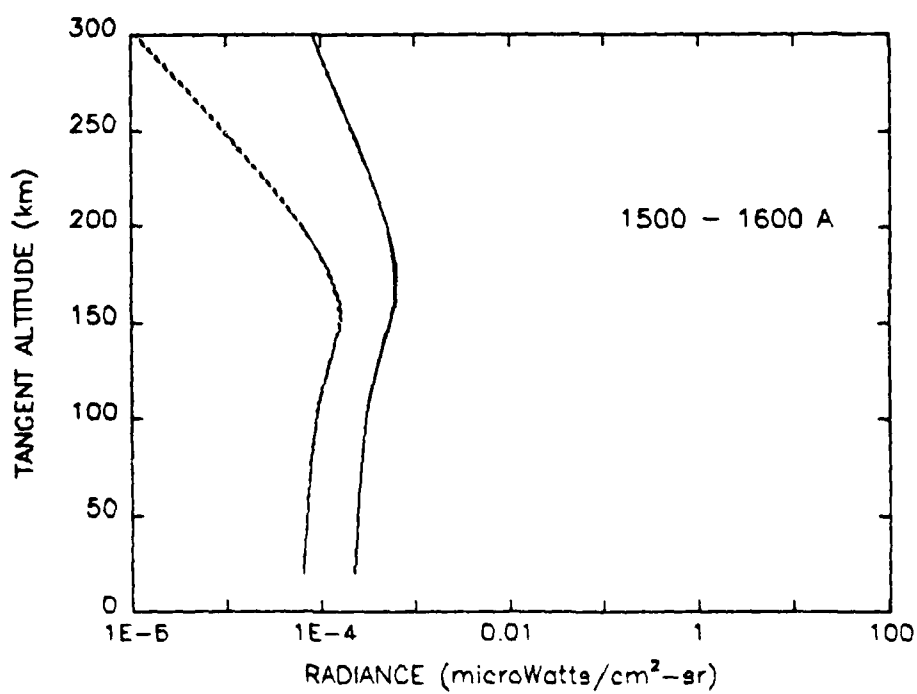
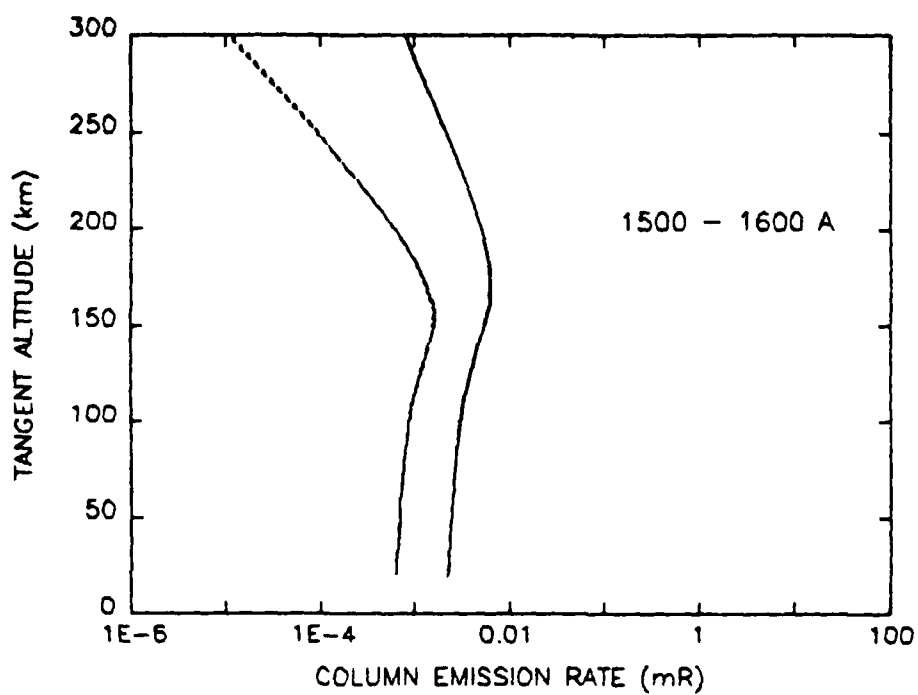


Figure 10. Similar to Figure 9 except from 1500 to 1600 Å

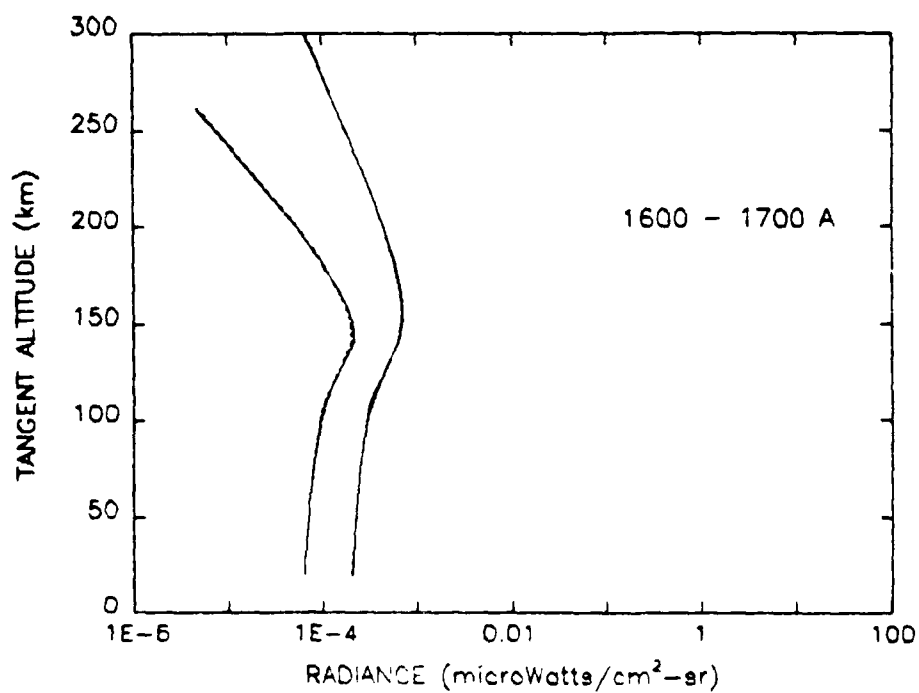
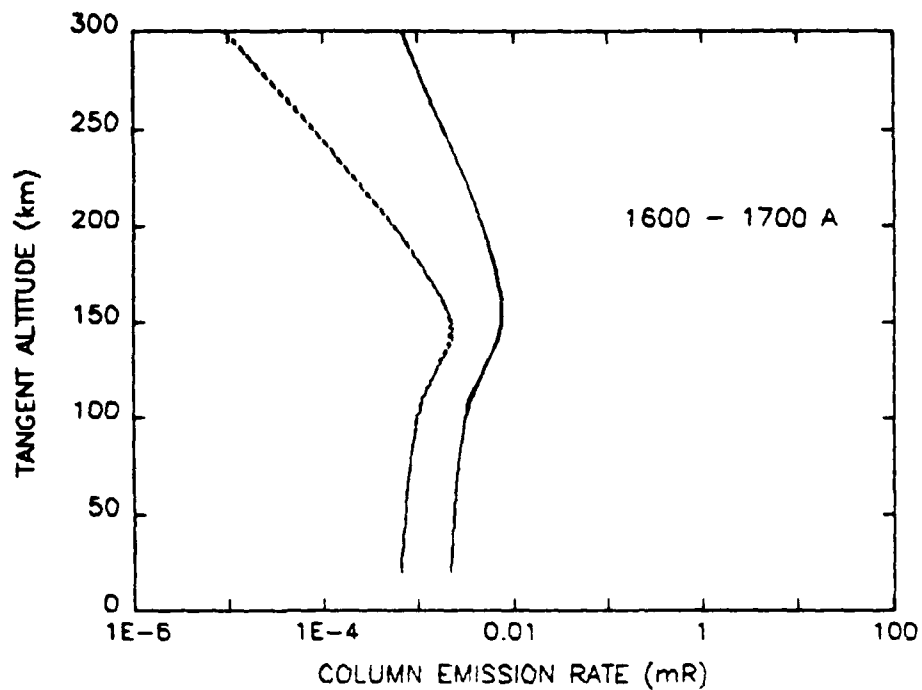


Figure 11. Similar to Figure 9 except from 1600 to 1700 Å

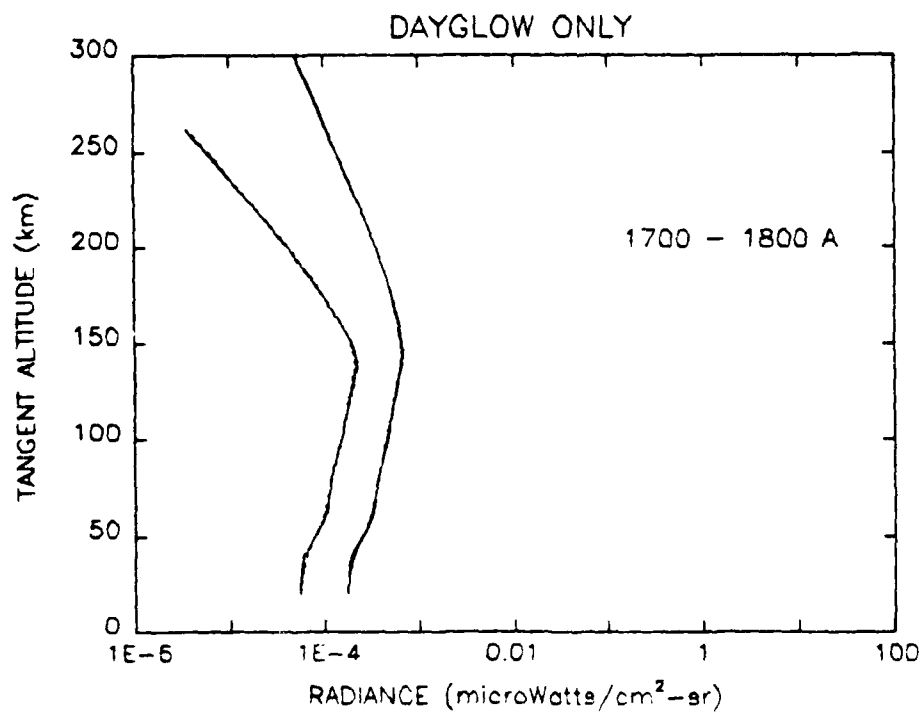
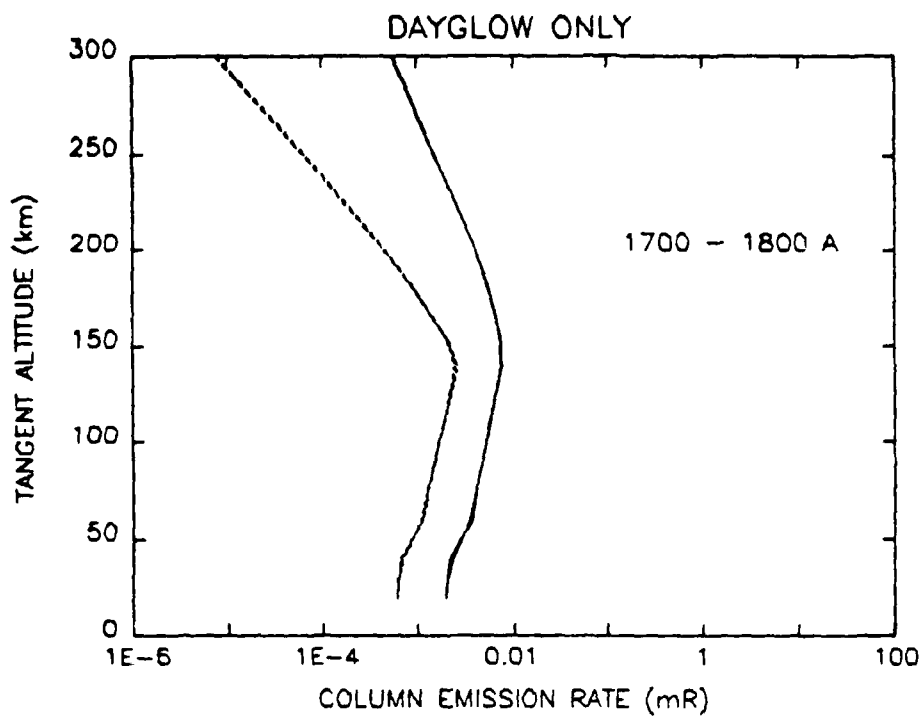


Figure 12. Similar to Figure 9 except from 1700 to 1800 Å. Rayleigh scattering begins to appear in this band but has not been included in this figure.

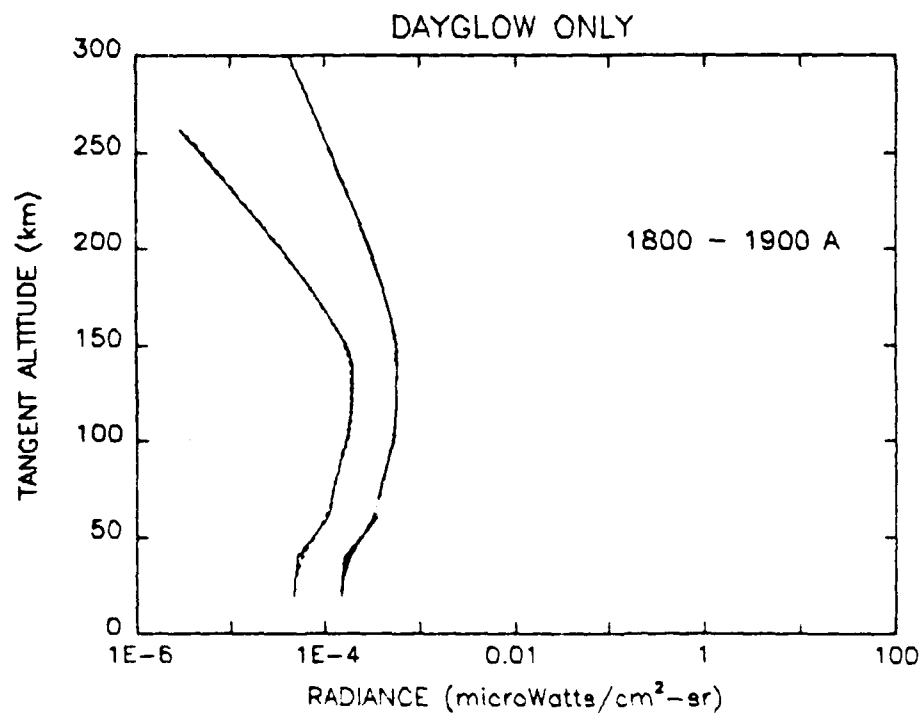
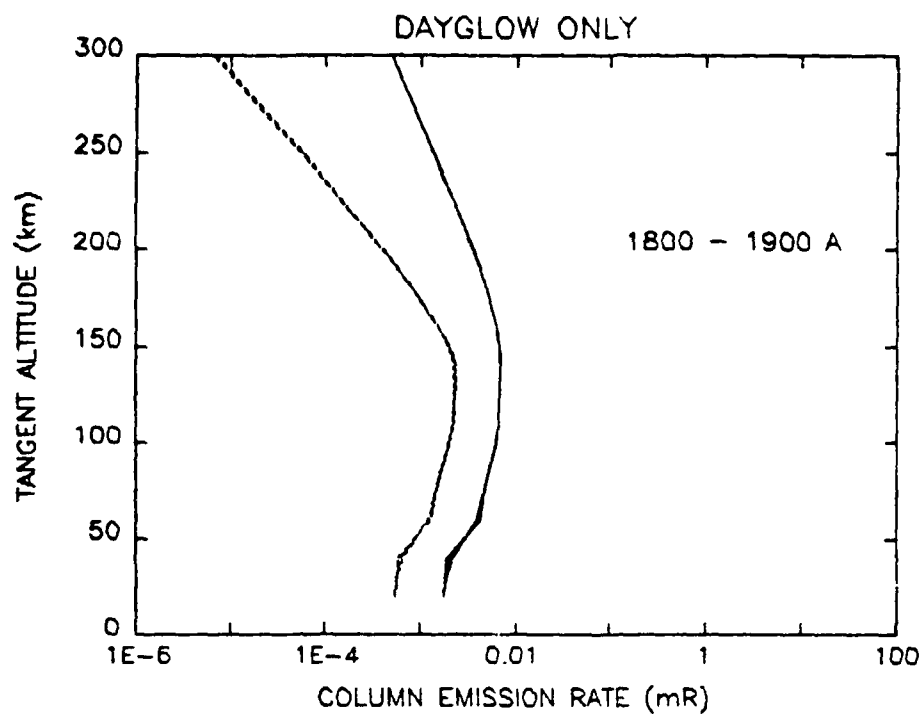


Figure 13. Similar to Figure 12 except from 1800 to 1900 A

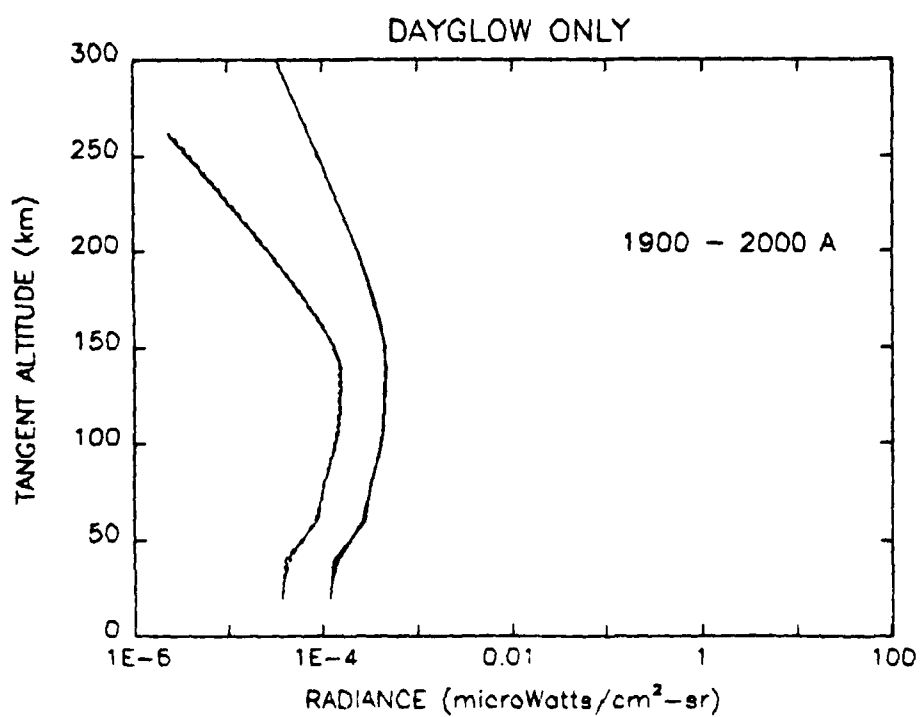
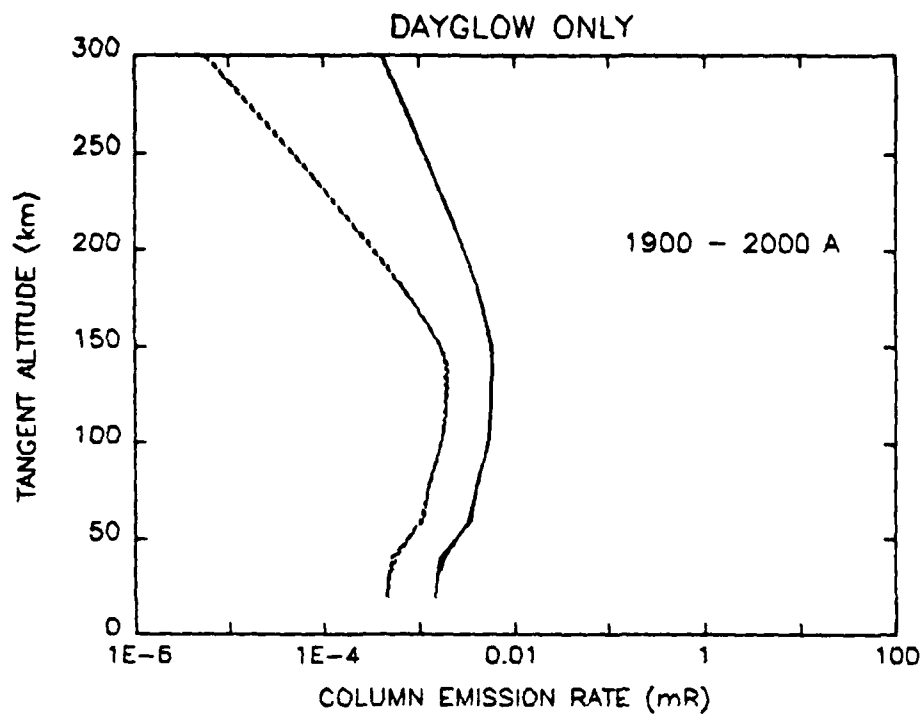


Figure 14. Similar to Figure 12 except from 1900 to 2000 A

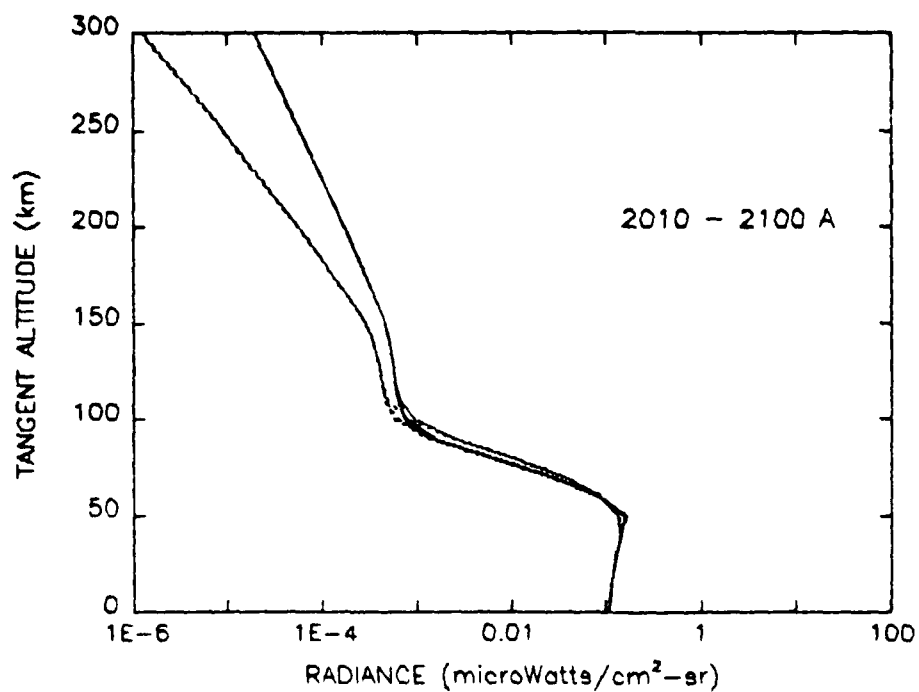
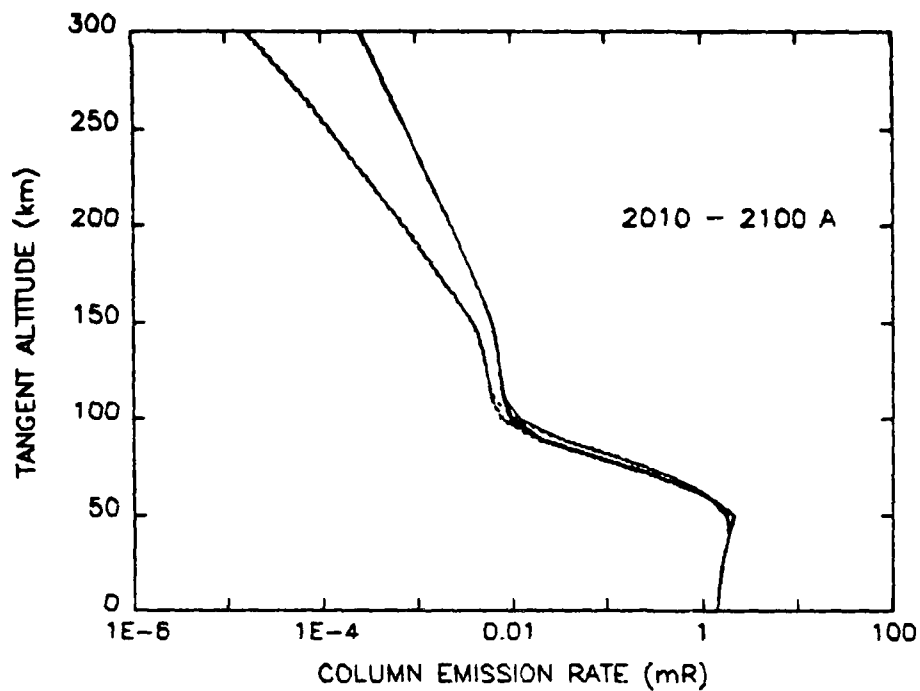


Figure 15. Similar to Figure 9 except from 2000 to 2100 A with the addition of Rayleigh scattering

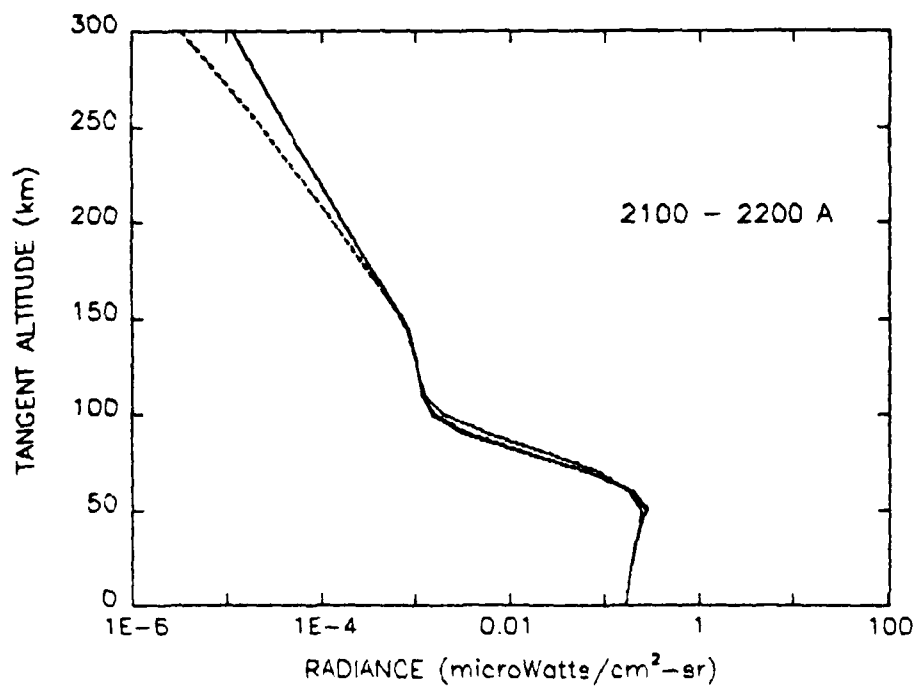
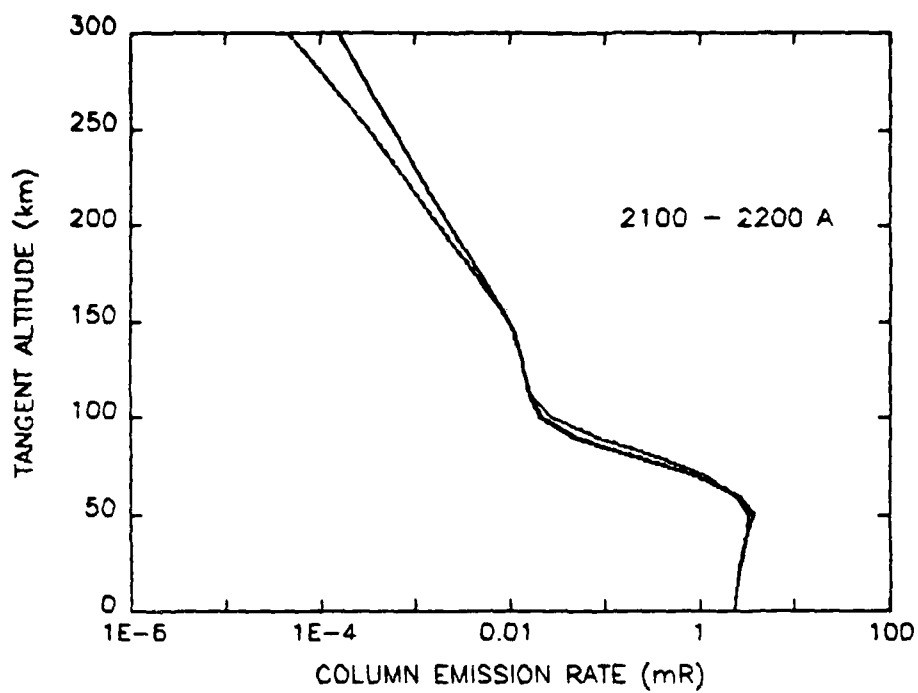


Figure 16. Similar to Figure 15 except from 2100 to 2200 Å

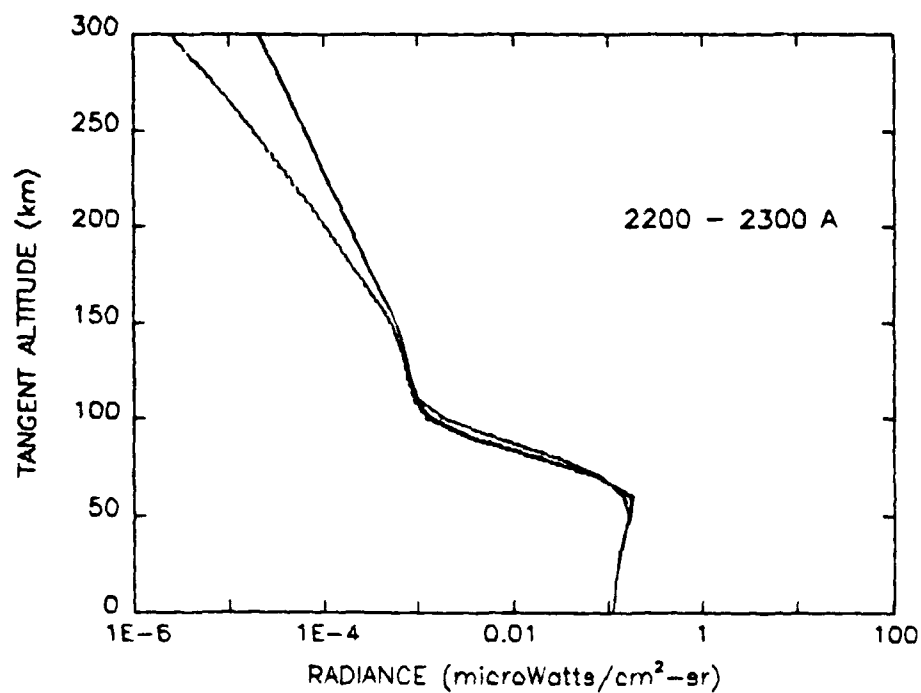
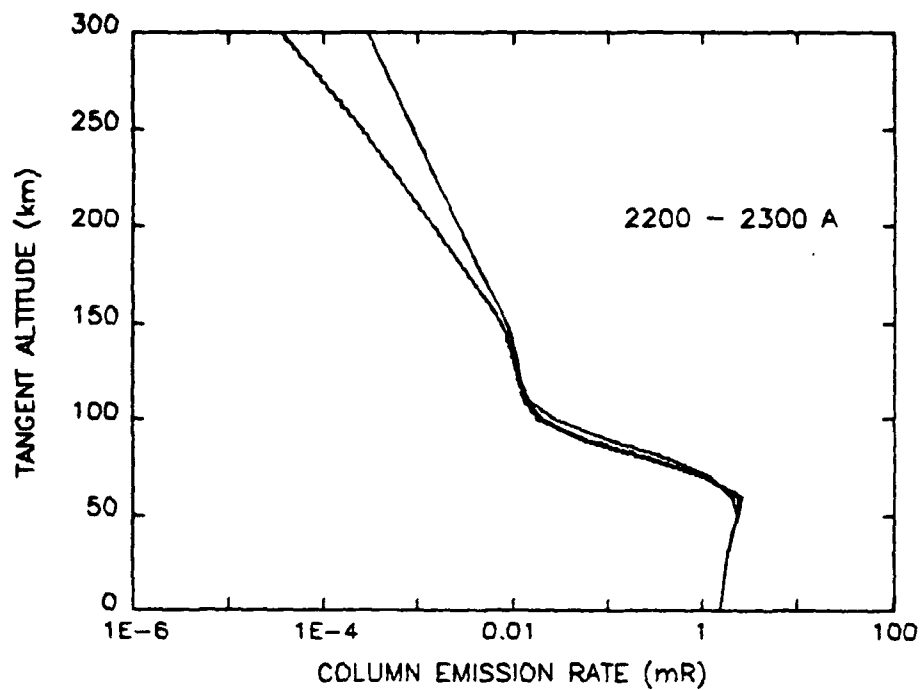


Figure 17. Similar to Figure 15 except from 2200 to 2300 Å

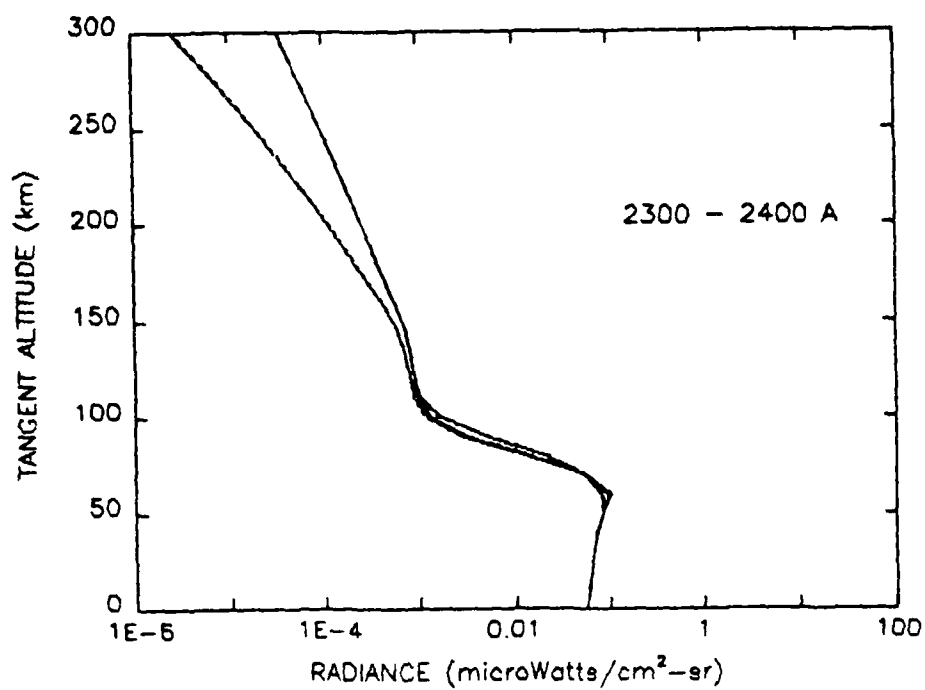
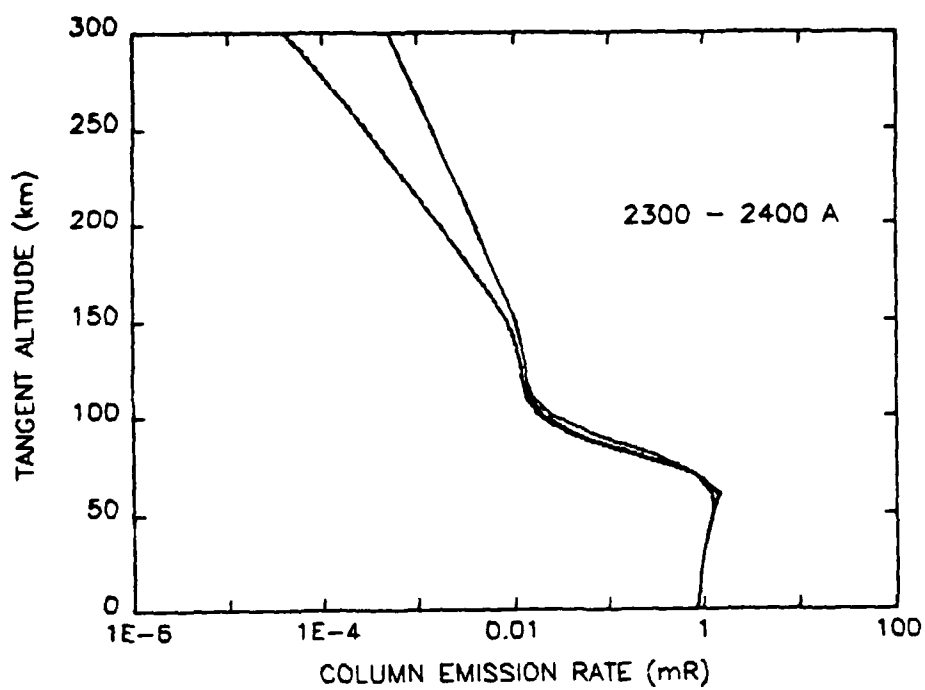


Figure 18. Similar to Figure 15 except from 2300 to 2400 Å

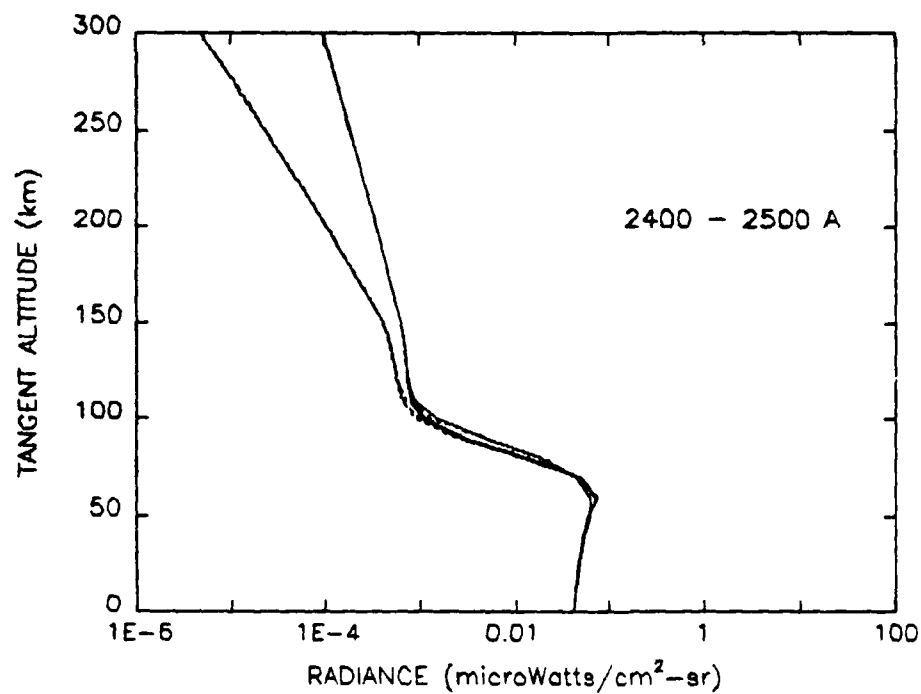
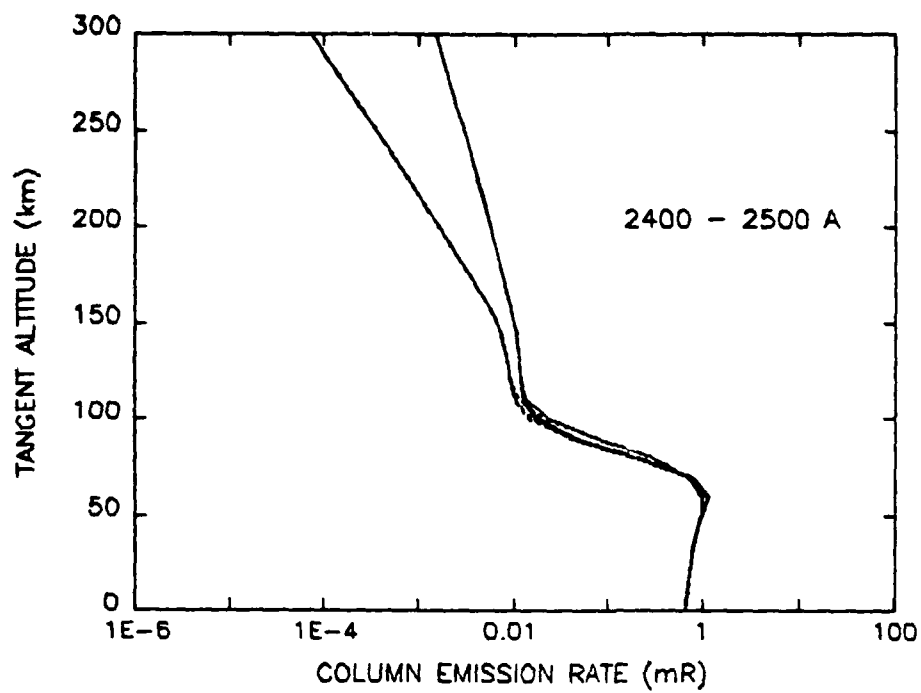


Figure 19. Similar to Figure 15 except from 2400 to 2500 Å

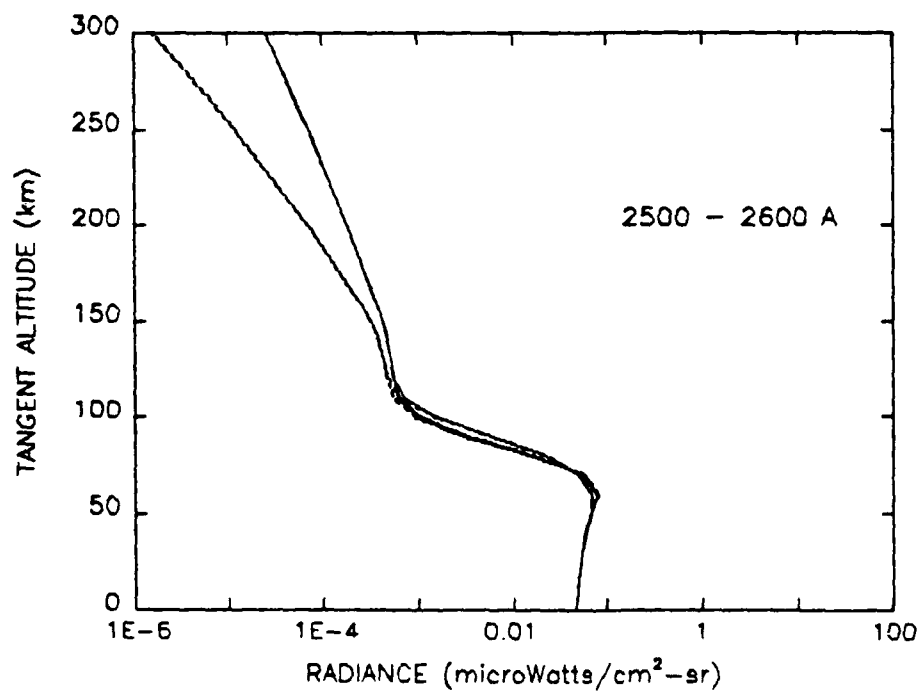
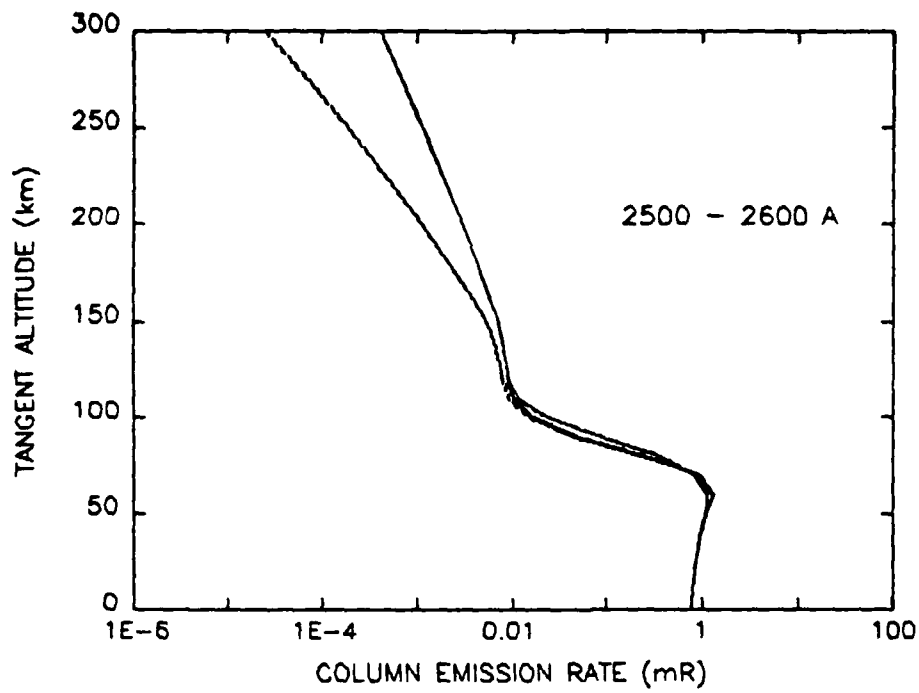


Figure 20. Similar to Figure 15 except from 2500 to 2600 A

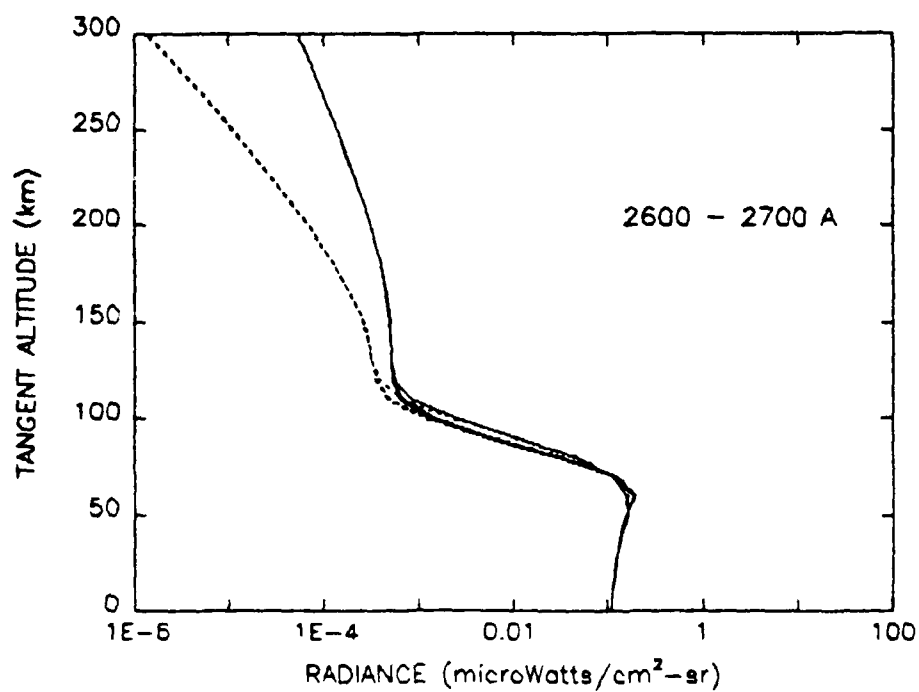
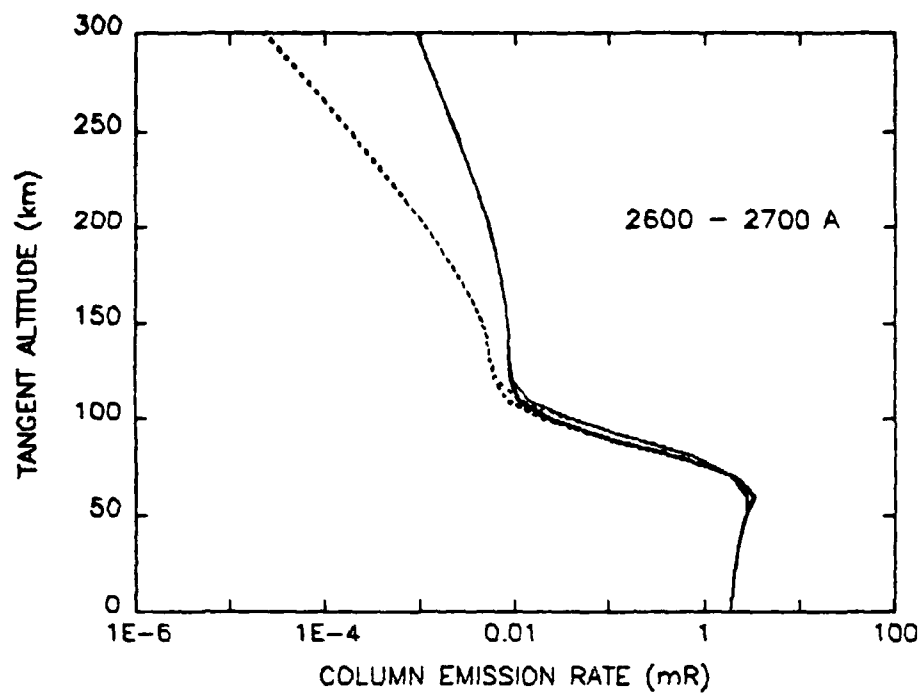


Figure 21. Similar to Figure 15 except from 2600 to 2700 Å

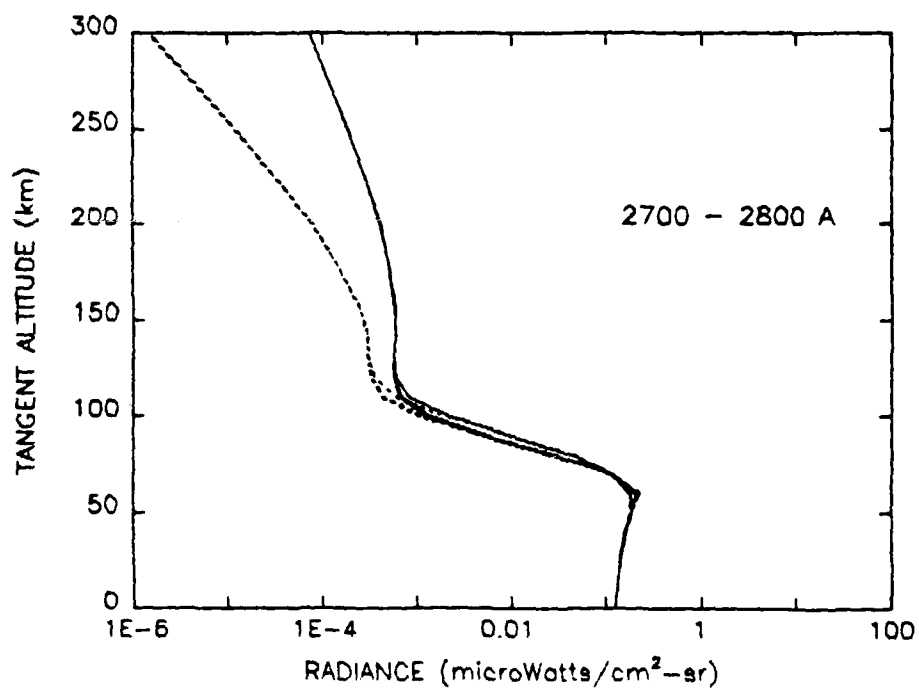
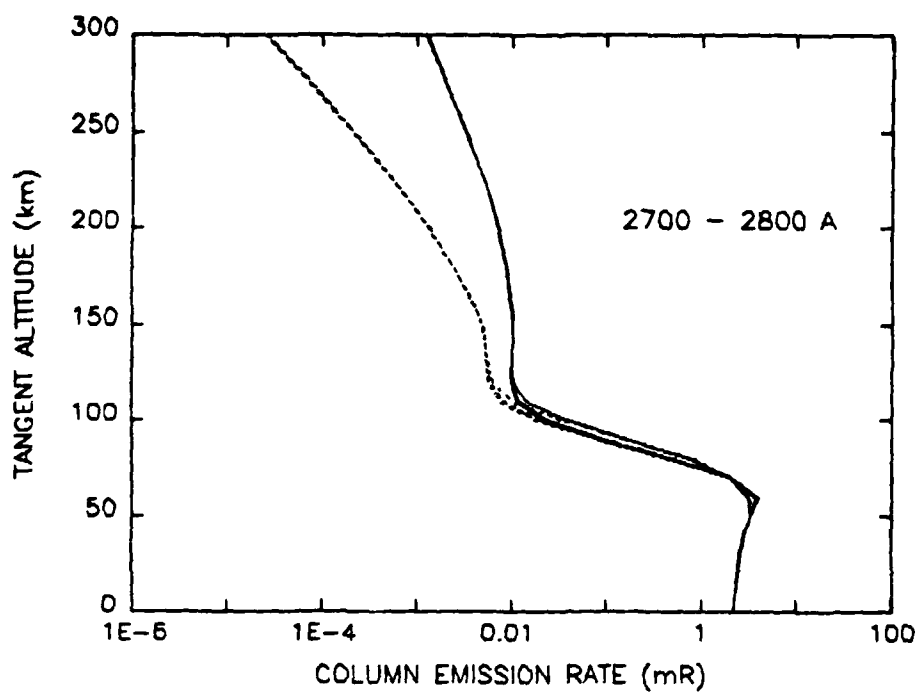


Figure 22. Similar to Figure 15 except from 2700 to 2800 A

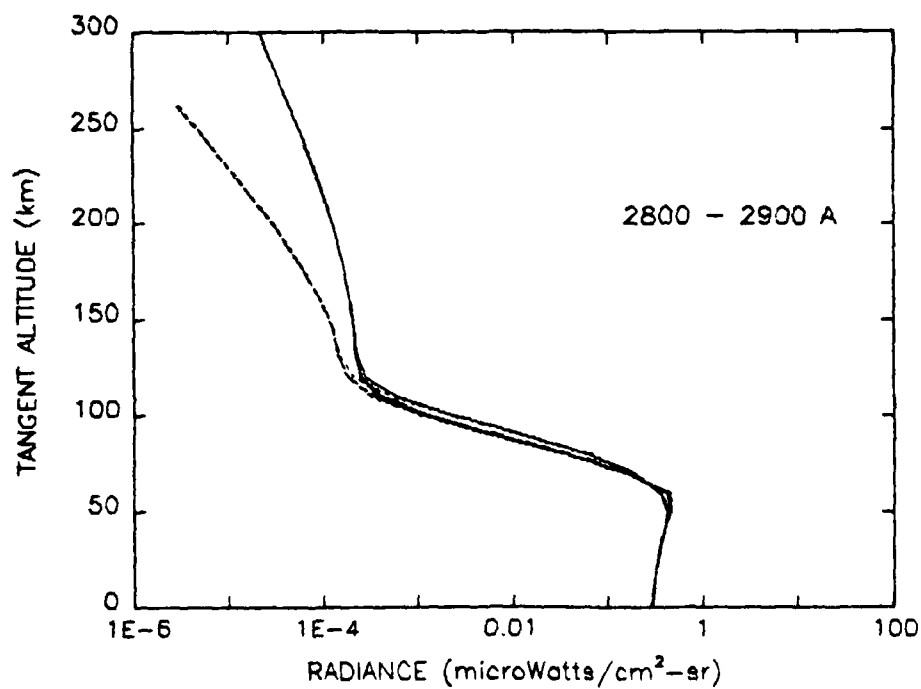
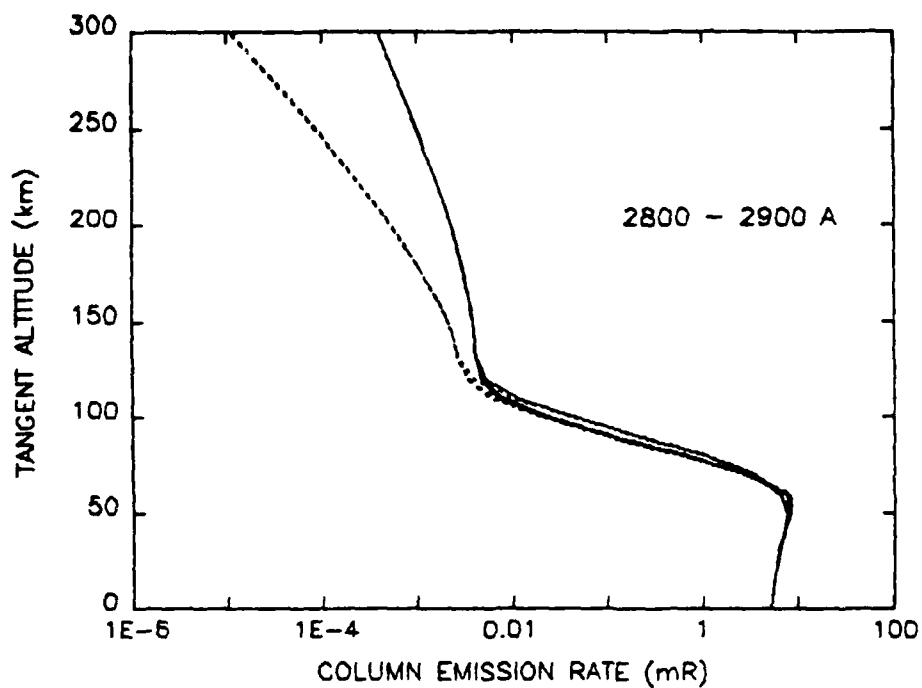


Figure 23. Similar to Figure 15 except from 2800 to 2900 Å

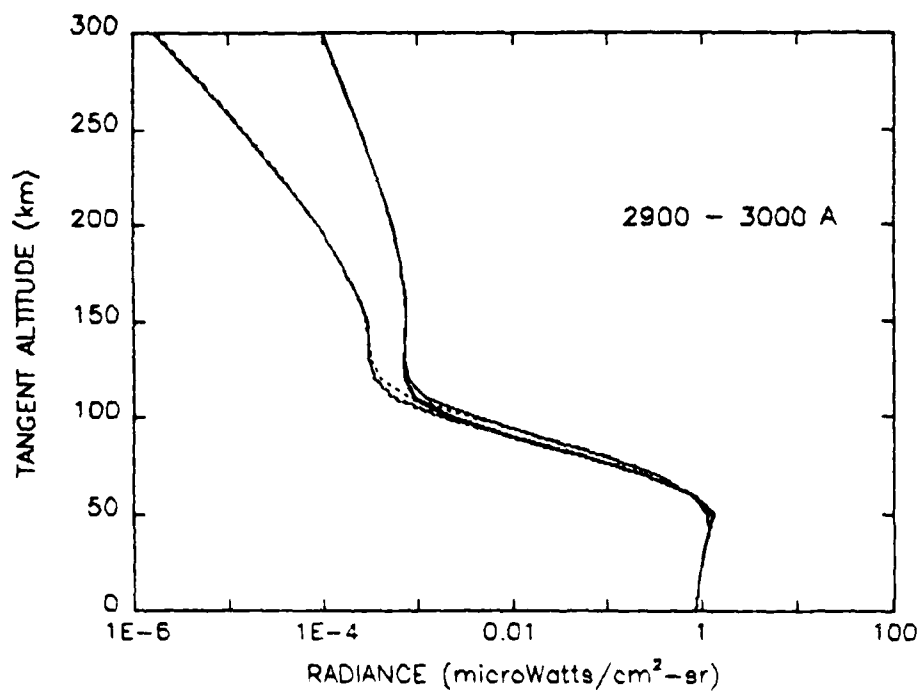
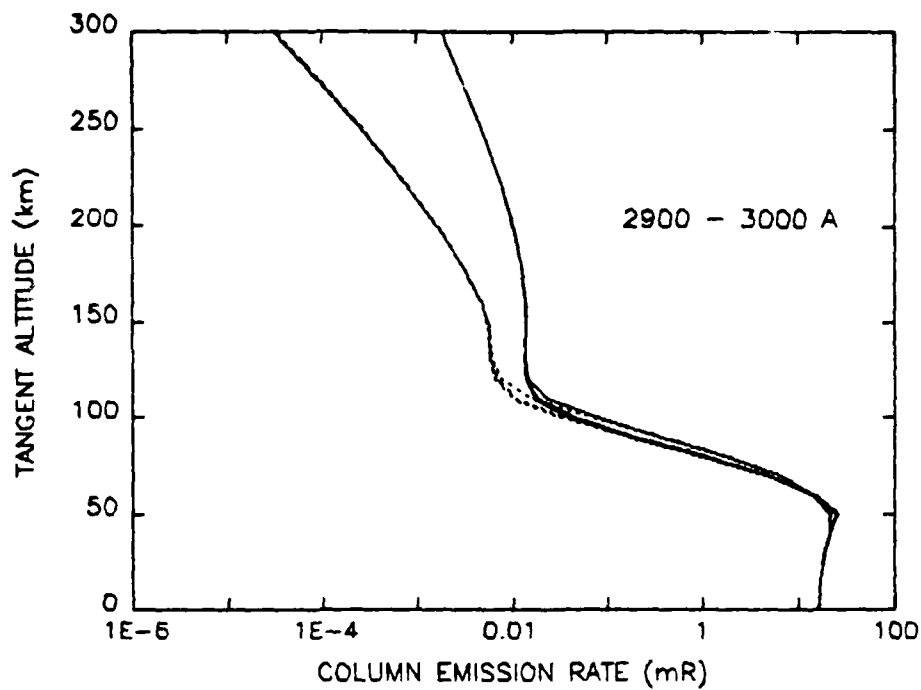


Figure 24. Similar to Figure 15 except from 2900 to 3000 A

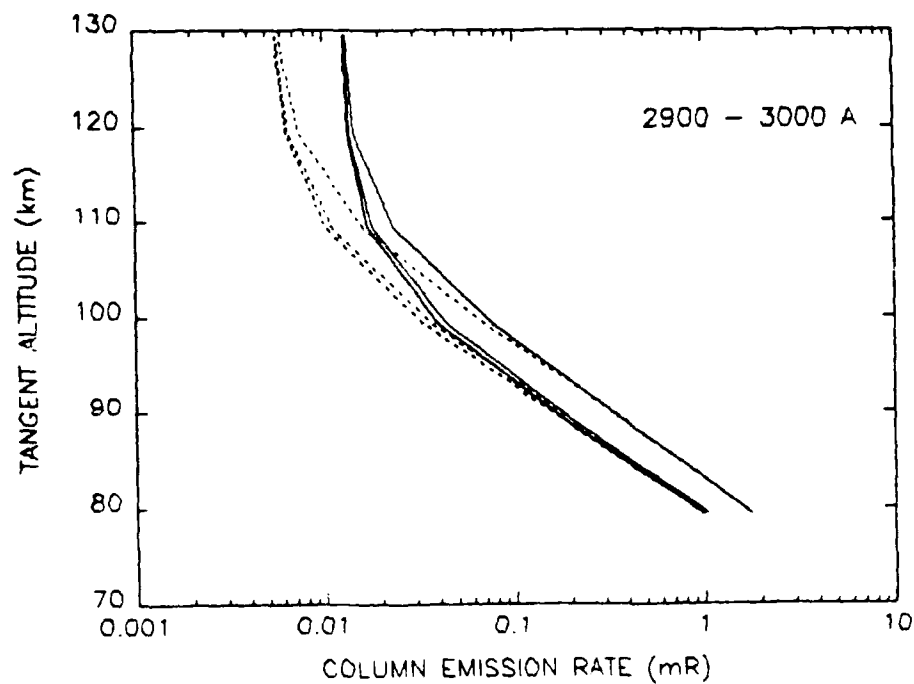
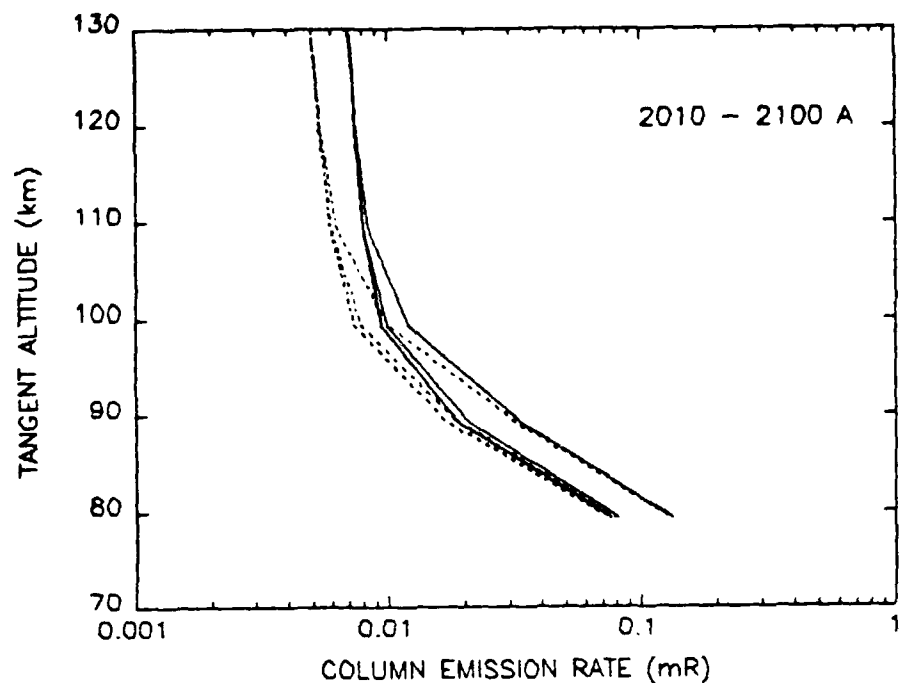


Figure 25. Limb profiles from Figs. 15 and 24 shown in greater detail around the 100 km tangent point

described by the Rayleigh phase function, which in normalized form is

$$p(\theta) = \frac{3}{16\pi}[1 + \cos^2\theta]$$

where θ is the scattering angle and integration over 4π gives unity. Figure 26 provides a sketch of the geometry illustrating how θ changes with the sun's azimuth. The largest deviation in the calculated intensity from the isotropic result occurs for single scattering. In this case the source function $S = S_0$ with the above angular dependence and the angle θ relates exclusively to the sun's direction which introduces a dependence of the sun's azimuth angle for a given elevation or solar zenith angle. The intensity for this situation is easy to calculate within our model and will be shown shortly for selected wavelengths. As scattering increases, S becomes magnified relative to S_0 , approaches isotropy for which $p(\theta) = 1/4\pi$ and thus ceases to have any dependence on the sun's azimuth angle.

As a first step in examining the effect of varying the sun's azimuth angle, we have separated S into two parts. They are S_0 and $S-S_0$. As mentioned above, the Rayleigh phase function is applied to S_0 . Isotropy is applied to $S-S_0$ which becomes increasingly accurate as the overall magnitude of S increases relative to S_0 . The intensity equation then becomes

$$I(\theta) = \frac{3}{16\pi}[1 + \cos^2\theta]I_{S_0} + \frac{1}{4\pi}I_{S-S_0}$$

which has been applied to obtain the results to follow.

Figures 27 - 29 present limb profiles for Rayleigh scattering based on the above equation for the wavelength intervals 2000-2100 Å, 2400-2500 Å and 2900-3000 Å. We have chosen a solar zenith angle of 60° rather than 30° here to achieve a greater range of azimuth angles. The full range is 30° to 150° but can be effectively taken from 30° to 90° since the phase function yields identical results from 90° to 150° . The top panels in these figures show the separate components due respectively to S_0 and $S-S_0$. For the wavelength intervals chosen, we observe that single scattering dominates over multiple scattering. This is true until reaching

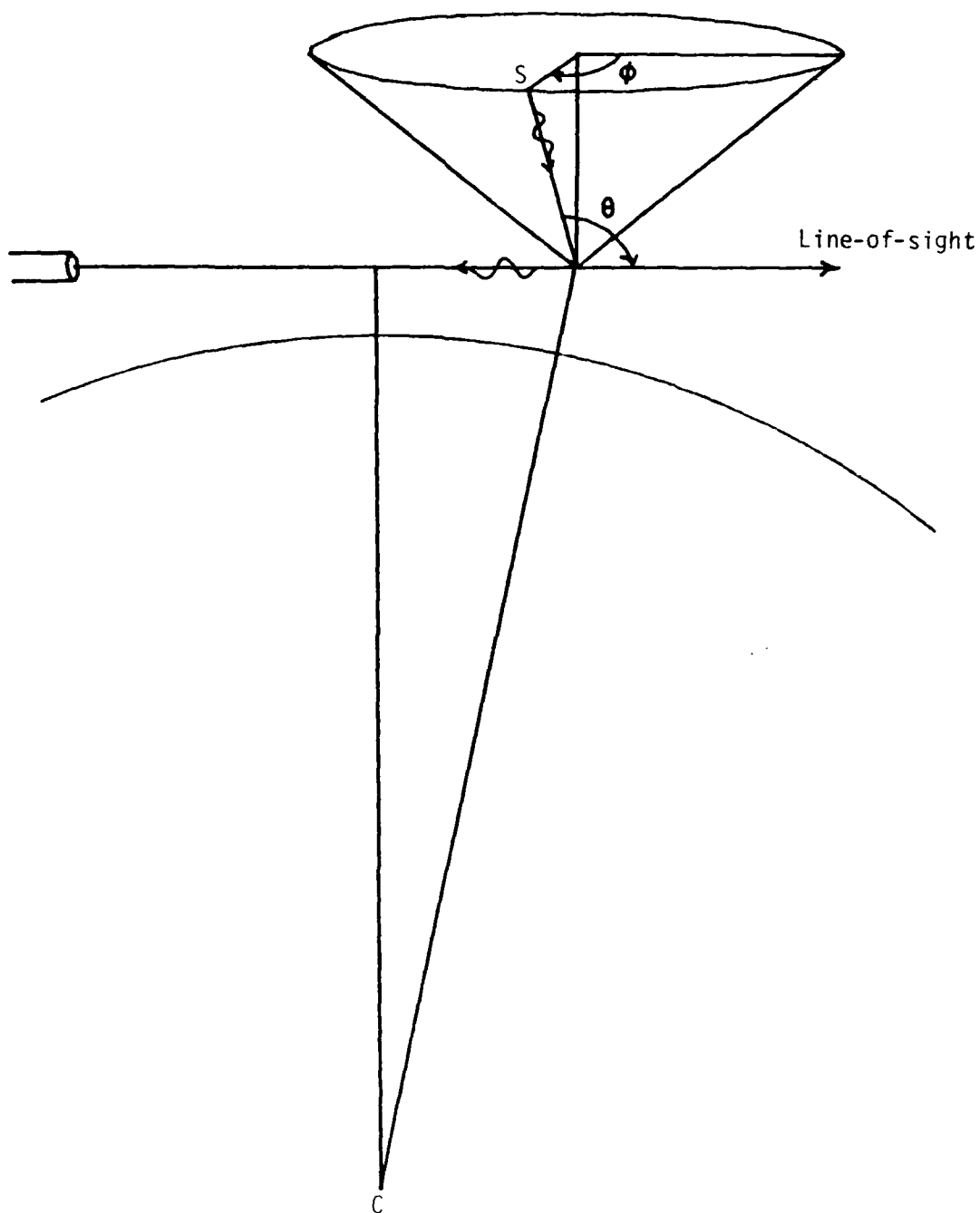


Figure 26. Geometry illustrating scattering angle θ in relation to the sun's azimuth ϕ .

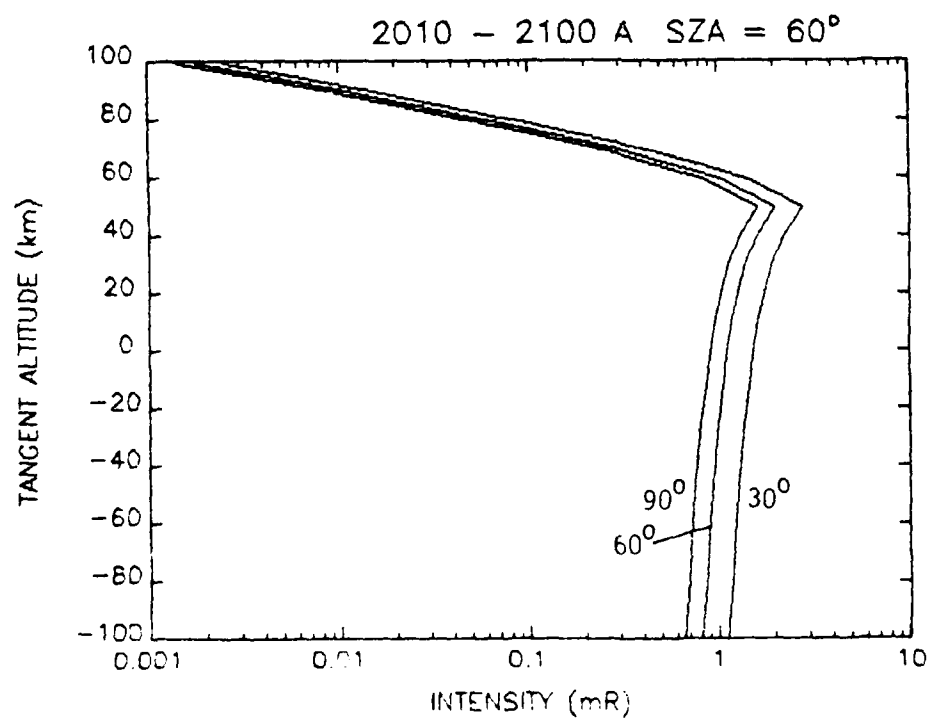
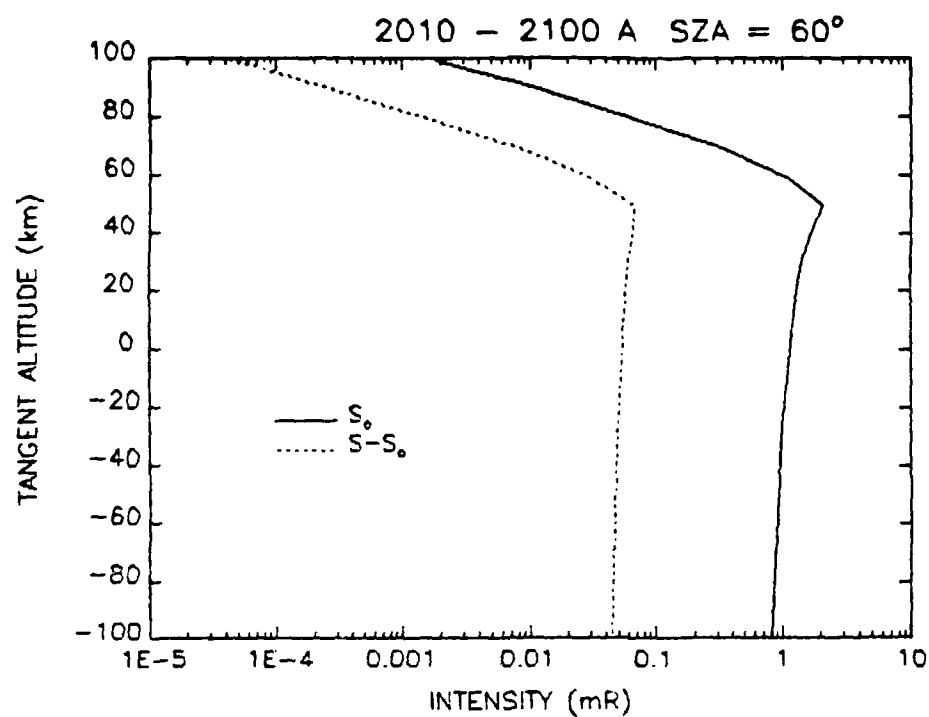


Figure 27. Limb profiles showing the effect of changing the sun's azimuth for the wavelength interval 2000 - 2100 Å. A given angle refers to the angle between the look and sun vectors.

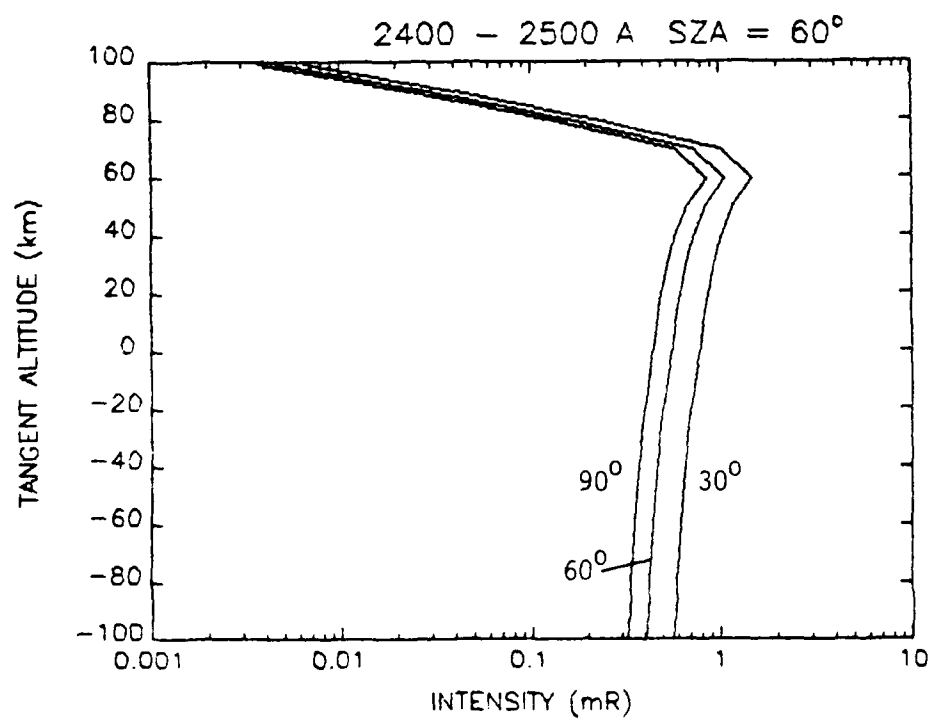
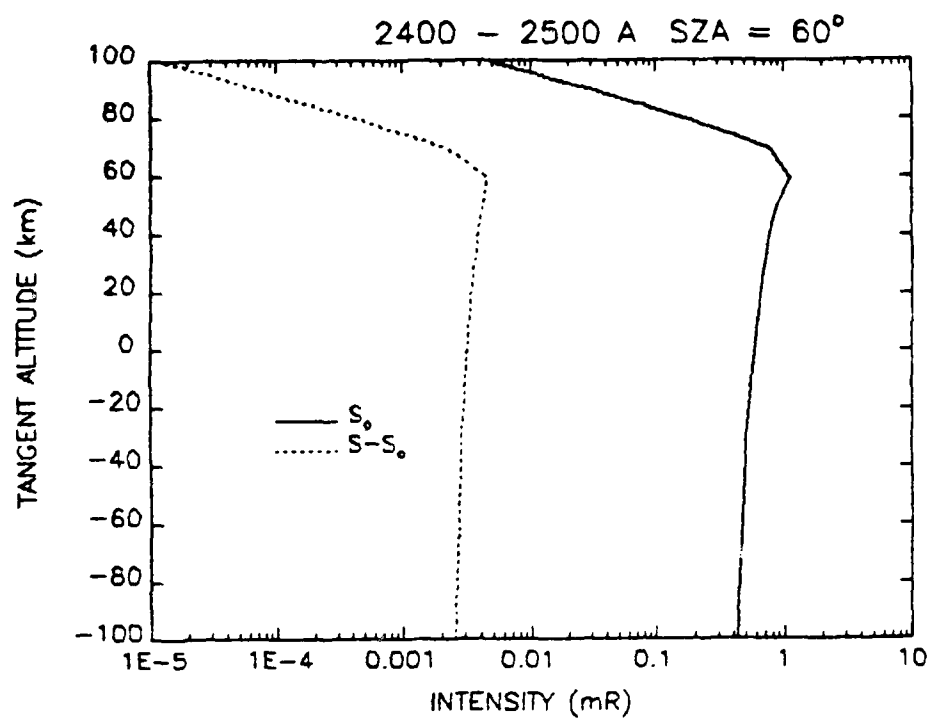


Figure 28. Similar to Fig. 27 except for the interval 2400-2500 Å

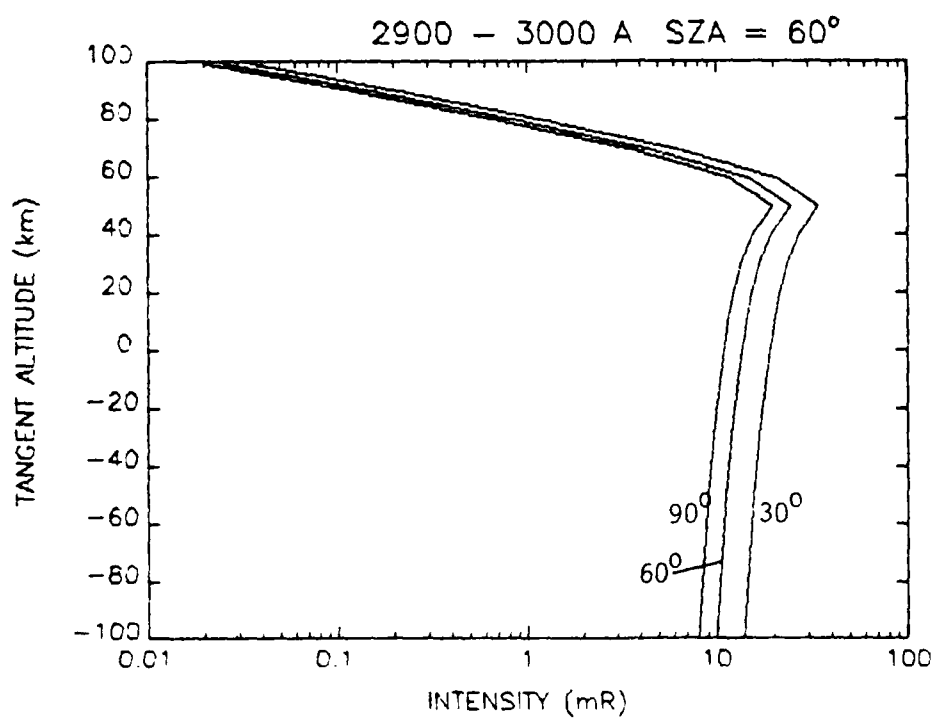
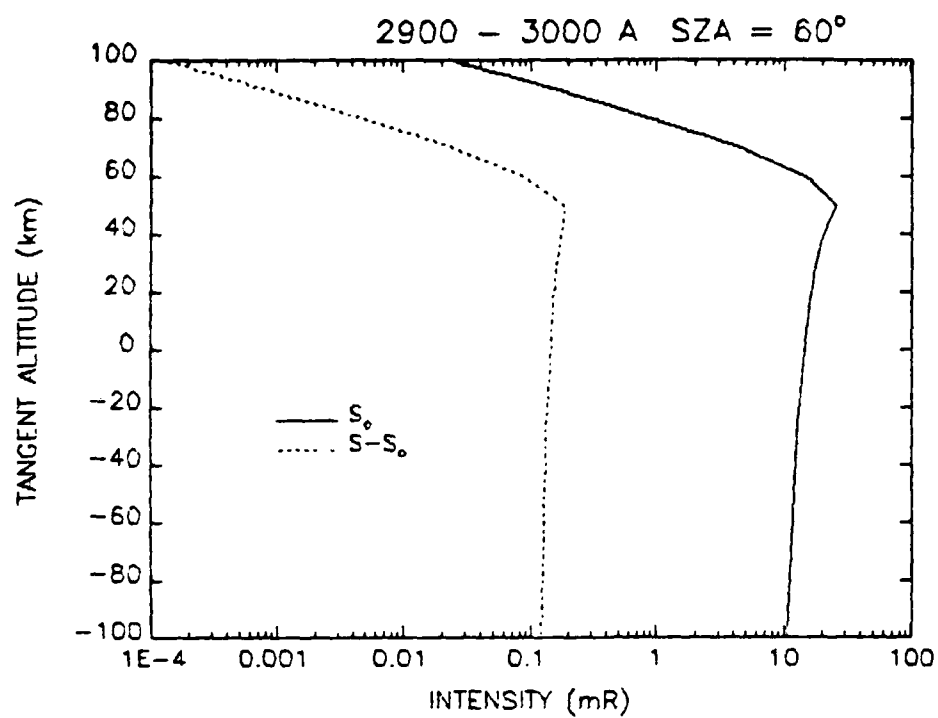


Figure 29. Similar to Fig. 27 except for the interval 2900-3000 Å

wavelengths longward of 3000 A at which point the full atmosphere is available for scattering and can produce S/S_0 ratios in excess of unity compared to values between approximately .1 and .01 shown in Figures 27 - 29.

The lower panels in the figures show how the upper panel components combine for azimuth angles of 30° , 60° and 90° . We see that an increase of nearly 1.75 is achieved going from 90° to 30° .

10. FUTURE DIRECTION

The following list gives some of the tasks we plan to pursue in the near future. The goal of these tasks is to strengthen and further test the model and to make predictions available to the community for sensor development, systems architecture and scene generation.

1. Compare with satellite data
2. Add features
3. Investigate the need to generalize the algorithm
4. Perform calculations both instrument specific and in standard brightness units with the latter being for generation of data bases.

The data obtained by AFGL's AIRS experiment on Polar BEAR and by various experiments on recent SDIO missions will be considered under item 1. Some of the features we wish to add are OI 1304 A, HI 1216 A and various systems and lines beyond 5000 A. The first two of these are presently in the model for one set of specific conditions as noted in Section 5. We will investigate the level of effort needed to adequately describe their variation as conditions such as solar activity and composition change. We are missing an important spectral region with regard to Rayleigh scattering, namely the Schumann-Runge band region from about 1750 to 2000 A. Approximate descriptions of the scattering in this region will be sought. Guidance to generalizing the algorithm will come from data analysis and comparisons with other models. In particular, selected comparisons are planned with LOWTRAN7 for nadir viewing to determine if improvements are needed in the Rayleigh scattering part of the algorithm from UV to visible wavelengths. If so, these improvements will likely concern our description of the background contribution coming from low altitudes and from the surface.

11. ACKNOWLEDGMENTS

This work was supported by funding from the Air Force Geophysics Laboratory through Dr. R. E. Huffman as part of the SDIO/SN ultraviolet phenomenology program.

12. REFERENCES

1. D. J. Strickland, D. L. Book, T. P. Coffey and J. A. Fedder, "Transport equation techniques for the deposition of auroral electrons", J. Geophys. Res., 81, 2755 (1976).
2. D. J. Strickland and D. E. Anderson, Jr., "Radiation transport effects on the OI 1356 A limb intensity in the dayglow", J. Geophys. Res., 88, 9260 (1983).
3. D. J. Strickland and R. R. Meier, "A photoelectron model for the rapid computation of atmospheric excitation rates", NRL Memo. Report 5004, Naval Research Laboratory, Washington, D.C. 20375 (1982).
4. R. R. Meier and J.-S. Lee, "An analysis of the OI 1304 A dayglow using a Monte Carlo resonant scattering model with partial frequency redistribution", Planet. Space Sci., 30, 439 (1982).
5. R. R. Meier, D. E. Anderson, Jr. and M. Nicolet, "Radiation field in the troposphere and stratosphere: I General analysis", Planet. Space Sci., 30, 923 (1982).
6. D. E. Anderson, Jr. and R. R. Meier, "The effects of anisotropic multiple scattering on solar radiation in the troposphere and stratosphere", Applied Optics, 18, 1955 (1979).
7. D. E. Anderson, Jr., R. R. Meier and J. B. Kumer, "Improved model of Mie scattering contribution to troposphere and stratosphere photodissociation fluxes", Applied Optics, 19, 1230 (1980).
8. D. E. Anderson, Jr., "The Troposphere-Stratosphere Radiation Field at Twilight: A Spherical Model", Planet. Space Sci., 31, 1517 (1983).
9. H. E. Hinteregger, "Representations of solar EUV fluxes for aeronautical applications", Adv. Space Res., 1, 39 (1981).

10. H. E. Hinteregger, K. Fukui and B. R. Gibson,
"Observational, reference and model data on solar EUV from
measurements of AE-E", Geophys. Res. Lett., 8, 1147
(1981).
11. A. E. Hedin, "A revised thermospheric model based on mass
spectrometer and incoherent scatter data: MSIS-83", J.
Geophys. Res., 88, 10170 (1983).
12. Atmospheric Ozone 1985, World Meteorological Organization
Report No. 16, NASA, Laboratory for Atmospheres, Code 614,
GSFC, Greenbelt, MD 20771 (1985).
13. R. P. McCoy, "Thermospheric odd nitrogen 2. Comparison of
rocket observations with a diffusive transport chemical
model", J. Geophys. Res., 88, 3206 (1983).
14. R. P. McCoy, Private Communication (1987).